Microwave Photonics Empowered Integrated Sensing and Communication for 6G

Lihan Wang, Xiangchuan Wang, and Shilong Pan, *Fellow, IEEE*
(Invited Paper)

***Abstract*— Integrated sensing and communication (ISAC) systems are gaining significant attention as a pivotal development direction for future 6G wireless networks. To overcome challenges related to bandwidth, resource reuse, and complexity inherent in traditional electronics, microwave photonics has emerged as a promising field for achieving high-performance ISAC. This article provides an overview of microwave photonic technologies in wireless communication and sensing, illustrating the performance enhancement brought by photonics. The recent progress and typical performance metrics of key technologies in microwave photonic ISAC, including microwave photonic ISAC frontend transceivers, resource multiplexing, integrated waveform design, and adaptive parameter adjustment, are highlighted. In addition, novel microwave photonic ISAC systems like holographic radio and distributed ISAC are discussed.**

***Index Terms*— Integrated sensing and communication (ISAC), integrated waveform design, microwave photonics, multiplexing technology, radio over fiber, 6G wireless network.**

I. Introduction

INTEGRATED sensing and communication (ISAC) is one of the fundamental scenarios for 6G wireless networks [1], offering significant application value in areas such as extended reality (XR) [2], the Internet of Things (IoT) [3], autonomous driving [4], robotic collaboration [5], and multisensory interconnection [6]. These emerging services demand not only high-speed communication but also precise positioning, high-resolution imaging, gesture recognition, and environmental monitoring [7], [8]. Given the need for numerous transmitters (Tx) and receivers (Rx) in 6G wireless networks, utilizing network nodes for direct sensing is highly promising [9], [10]. Fig. 1 illustrates a typical ISAC scenario enabled by 6G wireless networks. In outdoor environments, ISAC technologies provide high-quality communication for real-time data sharing while ensuring accurate sensing and positioning of users. For autonomous driving, existing radar and LiDAR technologies have limitations regarding sensing blind spots. By leveraging ISAC technologies, vehicle-to-everything (V2X) can be achieved, facilitating enhanced route planning and high reliability. In indoor conditions, small-scale base stations equipped with sensing capabilities can monitor individual status and enable collaboration between people and devices.

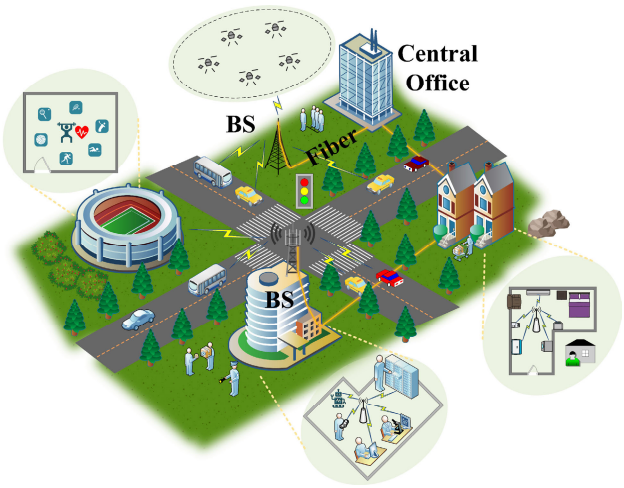

Fig. 1. Typical ISAC scenario based on 6G wireless networks.

The essence of ISAC lies in the reuse of hardware architecture and efficient resource sharing [7]. From a technical feasibility perspective, wireless communication and sensing align well in the following three aspects. First, communication and sensing can utilize the same channel, as they fundamentally involve transmitting information or detecting targets through wireless electromagnetic waves. This allows for the use of a common radio frequency (RF) frontend transceiver, including local oscillators (LOs), mixers, power amplifiers, and antennas. Second, existing communication and radar systems both employ techniques such as time-division multiplexing (TDM), frequency-division multiplexing (FDM), and multiple-input multiple-output (MIMO). This similarity suggests that the processes of signal transmission and processing can be fully integrated in theory. Finally, communication and sensing share a common objective of increasing carrier frequency and expanding available bandwidth. According to the Shannon theorem, channel capacity is proportional to the signal bandwidth for a given spectral efficiency. In practice, the transition from 3G to 5G has enhanced spectral efficiency through additional multiplexing techniques such as code

Received 23 October 2024; revised 22 December 2024; accepted 18 January 2025. Date of publication 4 February 2025; date of current version 15 August 2025. This work was supported in part by the National Key Research and Development Program of China under Grant 2022YFB2802704, in part by the National Natural Science Foundation of China under Grant 62271249 and Grant 62075095, in part by the Fundamental Research Funds for the Central Universities under Grant NC2024004 and Grant NI2023003, and in part by the Funding for Outstanding Doctoral Dissertation in Nanjing University of Aeronautics and Astronautics (NUAA) under Grant BCXJ24-09. *(Corresponding author: Shilong Pan.)*

The authors are with the National Key Laboratory of Microwave Photonics, Nanjing University of Aeronautics and Astronautics, Nanjing 210016, China (e-mail: andwwlh@nuaa.edu.cn; wangxch@nuaa.edu.cn; pans@nuaa.edu.cn).

Digital Object Identifier 10.1109/TMTT.2025.3532810

division multiple access (CDMA), orthogonal FDM (OFDM), and massive MIMO. In 6G, increasing bandwidth offers a viable approach to further boost the communication capacity. For sensing, the range resolution and accuracy are proportional to the signal's bandwidth and Gabor bandwidth, respectively. In complex ISAC scenarios such as V2X, the signal's bandwidth plays a crucial role in ensuring precise positioning, effective imaging, and large-capacity communication.

Traditional ISAC is implemented solely through electronic devices, which inevitably poses several challenges. One major issue is that existing electrical devices face limitations such as restricted bandwidth, poor tunability, hardware complexity, and electromagnetic interference (EMI) [11], making the generation and processing of high-frequency, wideband wireless signals difficult. Another concern is that as more devices connect to the 6G wireless network and seamless coverage becomes essential, the number of base stations will need to increase significantly [12]. Optimizing these base stations in terms of size, weight, power, and cost (SWaP-C) within the current architecture remains a pressing challenge. In addition, the sheer volume of data generated by numerous communication and sensing devices presents serious obstacles to the existing digital signal processing architecture [13].

Microwave photonics [14], [15] is an emerging interdisciplinary field that facilitates the generation, transmission, and processing of microwave signals in the optical domain [16]. This field exhibits several unique features compared to traditional electronics. While microwave devices and systems typically function at wavelengths ranging from centimeters to millimeters, optical signals operate at micrometer-scale wavelengths. Consequently, a broadband signal in the microwave domain can be regarded as narrowband from a photonic perspective. This allows optical devices to provide highly consistent and flat responses over a wide frequency range. Given that microwave signals from different frequency bands have distinct physical properties, a unified microwave photonic system capable of handling the entire microwave spectrum can significantly simplify system complexity. Moreover, integrated photonic chips can accommodate a combination of waveguides, modulators, and filters within a small footprint, thanks to the micrometer scale wavelength of optical signals. Recent advancements in integrated microwave photonics [17] have demonstrated significant potential in both communication [18], [19] and sensing [20], [21], paving the way for novel solutions in ISAC. In terms of signal transmission, optical fibers feature extremely low transmission losses (∼0.2 dB/km), lightweight (∼60 g/km), low cost, and resistance to EMI, making large-scale distributed systems feasible. Photonics also offers diverse resources, such as polarization, wavelength, and mode, which can be multiplexed for parallel signal processing and transmission. In addition, nonlinearity in optical and optoelectronic devices can be used to implement certain digital signal processing tasks, reducing computational load and decreasing the dependency on high-performance digital signal processors (DSPs). These characteristics make microwave photonics a promising and exciting field for application in ISAC.

This article reviews ISAC technologies for 6G wireless networks based on microwave photonics, highlighting the advantages, theoretical principles, typical system architectures, implementation approaches, and performance of the photonics-based ISAC systems. The structure of this article is as follows. Section II briefly introduces potential applications of microwave photonics in 6G wireless communication and sensing systems. Section III covers recent advancements in ISAC using microwave photonic technologies, focusing on four aspects: microwave photonic ISAC frontend transceivers, resource multiplexing, integrated waveform design, and adaptive parameter adjustment. Finally, Section IV concludes with a discussion of microwave photonic ISAC technologies and future prospects.

II. Typical Microwave Photonic Systems for Wireless Communication and Sensing

A. Wireless Communication

In the current 5G fronthaul network [22], the Cloud Radio Access Network (CRAN) architecture facilitates the connection between the wireless air interface and the fiber network. Remote radio heads (RRHs) are deployed close to the user equipment, while baseband units (BBUs) are centralized in cloud data centers. The connection between RRHs and BBUs is established via fiber links. This architecture allows for the deployment of distributed antennas within a cell [23], [24], reducing the uplink and downlink transmit power required for maintaining fixed channel quality and providing consistent service quality throughout the network. As CRAN evolves [25], future advancements in cooperation among RRHs may enable cell-free MIMO systems, in which a large number of distributed RRHs cooperatively serve all user equipment (UE) using coherent joint transmission. This distributed approach transforms mutual interference between each cell into useful signals, further enhancing both spectral and power efficiency. Within this framework, key issues include how to further increase the communication rate of base stations, reduce communication latency, avoid RF distortion, and lower the SWaP-C of base stations. Microwave photonics holds promise for resolving these issues in 6G networks, offering innovative solutions that enhance the efficiency and effectiveness of 6G wireless networks.

Building on the latest advancements in microwave photonics, Fig. 2 shows a conceptual architecture for a 6G base station using microwave photonics. This architecture primarily focuses on the downlink for simplicity. The BBU utilizes microwave photonic technology to directly generate high-frequency air interface signals. These generated signals are then transmitted to the RRH via a radio-over-fiber (RoF) link. At the RRH, microwave photonic beamforming technology is employed. In this subsection, we will review the latest developments in the three photonics-based technologies.

1) RF Generation: In 5G, frequency bands such as sub-6, 39, and 60 GHz are utilized to enhance communication capacity. As we transition into the 6G era, the demand for wireless air interface rates is expected to reach 100 Gbit/s and potentially scale up to 1 Tbit/s, which will require

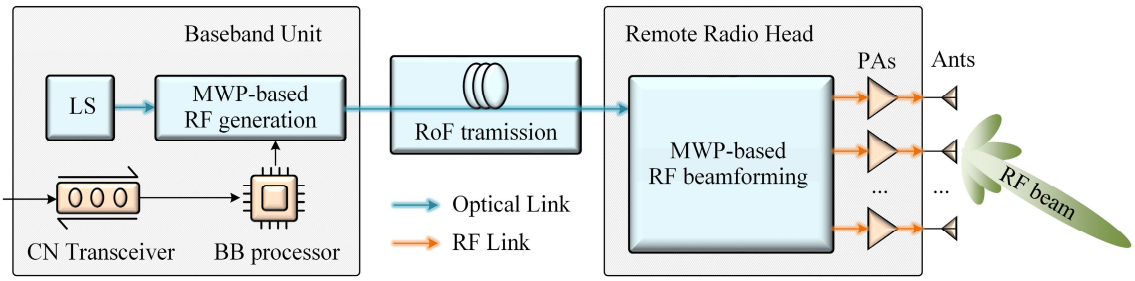

Fig. 2. Schematic of a microwave photonic 6G base station. CN, core network; BB, baseband; LS, laser source; MWP, microwave photonics; RoF, radio-over-fiber; RF, radio frequency; PA, power amplifier; Ant, antenna.

TABLE I
REPRESENTATIVE STUDIES OF MWP-BASED WIRELESS COMMUNICATION SIGNAL GENERATION

Multiplexing technique	Center Frequency	Wireless air interface rate	Wireless distance
None [26]	92.5 GHz	466.4 Gbit/s	6 m
None [27]	318 GHz	128 Gbit/s	0.02 m
None [28]	81 GHz	60 Gbit/s	1.2 m
None [29]	88.5 GHz	103 Gbit/s	4.6 km
None [30]	231 GHz	240 Gbit/s	5 m
2×2 MIMO [31]	300 GHz	137 Gbit/s	200 m
3×3 MIMO [32]	60.5 GHz	128.6 Gbit/s	7 m
3 WDM [33]	300 GHz	202.5 Gbit/s	30 m
80 WDM [34]	325 GHz	6.4 Tbit/s	54 m
PDM [35]	57.2 GHz	120 Gbit/s	1 m
PDM [36]	300 GHz	232 Gbit/s	200 m
PDM & 4 WDM [37]	124.5 GHz	1.056 Tbit/s	3.1m

expanding the air interface frequency spectrum. Microwave photonics offers promising approaches to simplify the architecture of high-frequency generation systems, avoiding the system complexity and signal degradation introduced by electrical frequency multipliers and mixers.

Table I highlights some of the most recent and notable studies on photonics-based wireless communication signal generation. These studies demonstrate that the generated wireless signals can cover the entire microwave frequency band, effectively overcoming the bandwidth limitations of traditional electronic devices. Moreover, the abundant resources available in the optical domain facilitate parallel transmission within a single fiber via techniques such as polarization-division multiplexing (PDM) and wavelength-division multiplexing (WDM). By leveraging these features, microwave photonics could support wireless air interface rates of several Tbit/s, which may propel the next generation of mobile communication. However, it is important to note that as frequency bands increase, power loss in the air interface also rises. To date, most research has concentrated on validating short-range wireless communication. Consequently, further investigation is required to explore methods for extending wireless communication distances and optimizing the efficiency of optical resources.

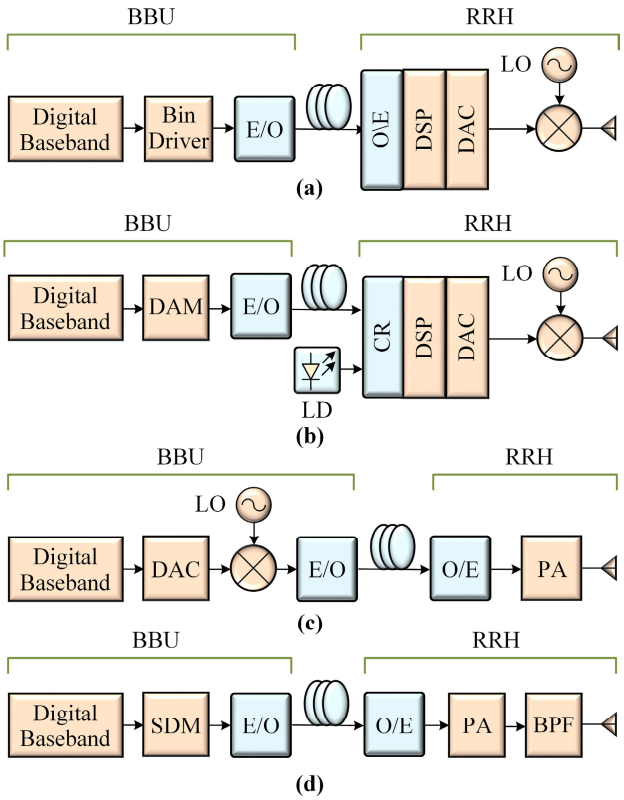

Fig. 3. Schematic of typical radio over fiber (RoF) links. (a) Digital RoF, (b) hybrid digital–analog RoF, (c) analog RoF, and (d) sigma–delta RoF. LD, laser diode; Bin, binary; E/O, electrical-to-optical; O/E, optical–to-electrical; DSP; digital signal processor; DAC, digital-to-analog converter; DAM, digital-to-analog modulation; CR, coherent receiver; SDM, sigma–delta modulation.

2) RoF Transmission: Current RoF technologies include digital RoF (DRoF), hybrid digital–analog RoF (DA-RoF), analog RoF (ARoF), and sigma–delta RoF (SD-RoF), as illustrated in Fig. 3. DRoF technologies, such as common public radio interface (CPRI) and its enhanced version (e.g., eCPRI), have been widely adopted in 4G and 5G networks. This technology digitizes the RF signals transmitted over the air interface into digital IQ data streams, taking advantage of the high fidelity of digital signals to ensure distortion-free transmission at rates typically ranging from 10 to 100 Gbps. Compared to traditional digital optical communication, the fronthaul network has a simpler internet protocol stack and a stricter latency requirement. However, the inherent nature of digital signals results in lower spectral efficiency.

To address this issue, hybrid DA-RoF technology has been developed [38], [39]. By transmitting the residual quantization error from DRoF in the analog form, spectral efficiency is significantly improved. Most DA-RoF systems utilize coherent reception, which enhances receiving sensitivity and can leverage optical polarization and phase resources to increase transmission capacity. Up to now, the most advanced hybrid DA-RoF technology can achieve a CPRI equivalent rate of 1 Pbit/s over a 2-km fiber fronthaul link [40]. Nonetheless, these methods require BBUs and RRHs to possess high-speed digital quantization capabilities. With the increasing number of wireless devices and rapidly growing demand for higher communication rates, it is anticipated that numerous high-performance analog-to-digital converters (ADCs) will be required at RRHs. In that case, current fronthaul networks may face significant challenges in terms of power consumption, cost, and transmission rates.

In contrast, ARoF technology can greatly simplify the structure of the RRH by directly transmitting RF air interface signals through the fiber, eliminating the need for the CPRI digital interface's quantization process. The RRH only requires the optoelectronic conversion devices and RF frontend transceivers, which significantly reduces complexity and costs. However, ARoF transmission faces significant challenges related to link nonlinearity and signal distortion, primarily caused by nonlinearities in the optoelectronic conversion process and noise within the link [41]. In addition, if RF signals are generated using optical heterodyning, phase noise from lasers must be mitigated [42], [43]. When transmitting multicarrier signals, a high peak-to-average power ratio (PAPR) can further exacerbate intermodulation distortion, leading to a reduction in the dynamic range of the link. To overcome these issues, it is crucial to develop high-linearity RoF links [44], [45], [46], [47]. Various techniques, such as analog predistortion [48], [49], digital predistortion [50], [51], and equalization algorithms [52], [53], [54], can be employed to address the link nonlinearity. Considering that ARoF-based wireless communication systems involve cascaded wireless channels and optoelectronic links, traditional modulation formats like OFDM, commonly used in 4G and 5G, may not be the most effective for ARoF systems. Alternatives such as universal-filtered multicarrier (UFMC) [55] and multiband carrier-less amplitude phase modulation (multi-CAP) [56] are worth exploring. To effectively realize cell-free massive MIMO under ARoF architecture, it is crucial to carefully consider RF distortions [57], [58].

Another approach to implementing RoF technology is SD-RoF [59], [60], which combines the nonlinearity resistance of DRoF with the structural simplicity of ARoF. This method generates digitally encoded signals modulated by sigma–delta at the BBU, requiring only simple optoelectronic conversion and filtering at the RRH to recover the RF signals. This significantly reduces the linearity requirements for RoF links, achieving a 40-dB reduction in the third-order intermodulation distortion compared to ARoF and improving error vector magnitude (EVM) several times [61]. Furthermore, experiments have validated its feasibility in distributed MIMO systems [62], [63], [64], enabling cost-effective collaborative communication and positioning.

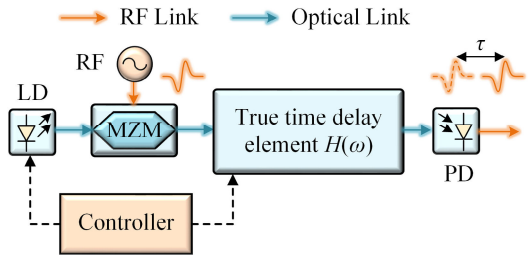

Fig. 4. Schematic of the typical optically-controlled true time delay system. MZM, Mach–Zehnder modulator.

3) Beamforming: Massive MIMO is a key technology in 5G, enabling precise control of electromagnetic waves in any direction and high directional gain through beamforming. Beam direction adjustments are implemented by controlling the phases of transmitted signals between antennas. However, wideband signals would cause beam squint issues, where the beam shifts from its intended direction [65], [66], [67]. Microwave photonic beamforming addresses this problem by modulating RF signals onto optical carriers, allowing delay control in the optical domain for each branch. Unlike traditional phased array techniques, microwave photonic beamforming offers true time delay (TTD) control that is frequency-independent, effectively resolving beam squint issues with a large tunable range and low transmission loss [68].

The typical optically-controlled TTD system is illustrated in Fig. 4. Assuming the TTD element has a frequency response $H(\omega)$, the phase difference introduced in the microwave photonic link can be expressed as [69]

$$\Delta\varphi(\omega_m) = \arg\{A_{-1}^* A_0 H^*(\omega_c - \omega_m) H(\omega_c) + A_0^* A_{+1} H^*(\omega_c) H(\omega_c + \omega_m)\} \quad (1)$$

where ω_m and ω_c denote the frequencies of the modulation signal and the laser, respectively, arg(.) represents the argument of a complex number, and A_n is the complex constant corresponding to the nth sideband of the modulated optical signal. To realize a TTD function, the following equation must be satisfied:

$$\frac{\mathrm{d}\Delta\varphi(\omega_m)}{\mathrm{d}\omega_m} = \tau, \quad \Delta\varphi(0) = 0 \quad (2)$$

where τ is the desired transmission delay.

Based on (1) and (2), microwave photonic beamforming [70] can be mainly divided into two types: switching the optical propagating path and adjusting the equivalent optical propagating path length. The first method relies on multistage optical switches connected to different waveguides [71], [72]. A discrete propagating delay tuning function is realized by changing the state of optical switches. To achieve delay tuning capabilities with a large range and high accuracy, the TTD network must increase the number of delay line stages, which complicates and destabilizes the beamforming network. Other microwave photonic beamforming methods circumvent this issue by utilizing the dispersion effect in the

optical waveguide to achieve continuous delay tuning [73]. Generally, the equivalent optical propagating path length can be adjusted by changing the dispersion coefficient of the link or the wavelength of the laser. One representative approach is an integrated tunable optical delay line scheme based on a microring resonator, where the beamforming network can be integrated into a mm^2-level footprint [74], [75], [76]. To mitigate the severe amplitude-phase coupling in a single microring resonator, we proposed a flat-top response microring based on manipulating the slow- and fast-light effects [77], [78]. The design achieves a tuning range exceeding 100 ps, with an amplitude variation of less than 0.8 dB. Such flat-top microring resonators are particularly promising for future integrated RF beamforming networks.

Morant et al. [79] introduced a microwave photonic beamformer using an integrated Si_3N_4 optical microring resonator for millimeter-wave communication. This system utilizes multicore optical fibers to distribute signals to different antenna elements. The microring resonator allows rapid tuning of the transmission delay by adjusting the laser wavelength. In experiments, the system transmitted a 128-quadrature amplitude modulation (QAM) signal with a bandwidth of 4.2 GHz at 17.6 and 26 GHz, achieving a data rate of 21 Gbit/s for a two-element system and 16.8 Gbit/s for a four-element system. To fully exploit the integration capability of microring resonators, Visscher et al. [80] proposed a fully integrated 1×4 microwave photonic broadband beamforming array system. This system employs thermally tuned microring resonators to form a delay line, providing 200 ps of continuously tunable delay over a 5-GHz bandwidth. All components, i.e., optical source, modulator, optically-controlled TTD network, and photodetector (PD), are integrated into a single chip. Subsequent studies investigated the system's performance by transmitting 500 Mbaud 16 QAM signals at 5 and 10 GHz, achieving error-free transmission within a $\pm 45°$ beam angle range.

B. Wireless Sensing

In 6G networks, we envision a wireless sensing scenario within a complex electromagnetic environment featuring multiple UE. Base stations need to detect the spatial locations of UE, reconstruct the surrounding environment, and identify available spectra. Based on the sensing results, a sensing-assisted communication function can be implemented. Base stations can dynamically adjust their operating frequencies and beams to enhance spectral and power efficiency while ensuring high-quality communication for users. Furthermore, the sensing results obtained from different base stations can be combined using information-level and signal-level fusion, improving the sensing range, resolution, and sensitivity. This is referred to as communication-assisted sensing.

Wireless sensing based on microwave photonics offers the ability to generate and process high-frequency and wideband signals, overcoming the bandwidth limitations of traditional electronic technologies. This allows for high-resolution environmental information sensing as well as wideband and real-time spectrum monitoring. The main research directions in microwave photonic wireless sensing, including ranging, imaging, positioning, angle-of-arrival (AoA) estimation, and spectrum sensing, are illustrated in Fig. 5. In recent years, extensive studies have been conducted in this field, and this subsection will provide an overview of these advancements.

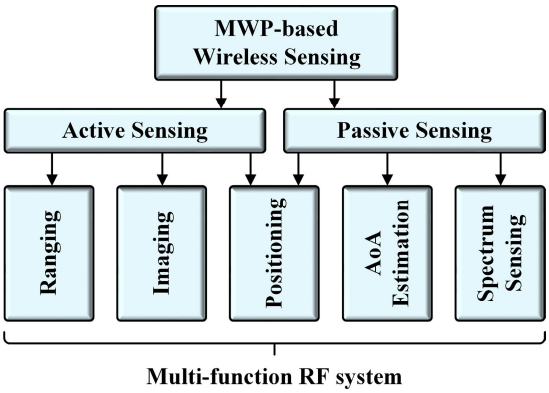

Fig. 5. Main research directions of wireless sensing based on microwave photonics. MWP, microwave photonic; AoA, Angle-of-arrival.

1) Ranging: Ranging is one of the fundamental functions in wireless sensing systems. It can be regarded as a typical parameter estimation problem. The ranging accuracy and resolution depend on the spectrum of the sensing signal, as described by the following equations:

$$\sigma_R^2 \geq \frac{c^2}{8\pi^2 \mathrm{SNR} \cdot \beta_s^2} \tag{3}$$

$$\Delta R = \frac{c}{2B} \tag{4}$$

where c is the speed of light, SNR is the signal-to-noise ratio (SNR) of the received signal, and β_s^2 and B denote the second moment of the signal spectrum and signal bandwidth, respectively.

Microwave photonics can easily generate high-frequency, wideband microwave signals, thereby providing superior ranging performance. Commonly used ranging signals include Gaussian pulses [81], chaotic signals [82], [83], and linear frequency-modulated (LFM) signals [84], [85], [86]. Among them, LFM signals are widely used in microwave photonic sensing systems due to their excellent pulse compression characteristics. Furthermore, LFM signals can be dechirp-received via microwave photonic mixing [87], [88], which converts high-frequency, wideband signals into low-frequency, narrowband dechirped signals. This transformation allows low-speed ADCs to sample the signals, reducing data volume and ensuring fast signal processing. In [89], an 8-GHz bandwidth LFM signal was converted into an MHz-level low-frequency signal through photonic dechirping, enabling a 2-cm range resolution in real-time operating mode. Wang et al. [90] utilized photonic in-phase and quadrature (I/Q) mixing to dechirp dual-band wideband LFM signals, and subsequently achieved rapid fusion processing of the dual-band dechirped signals, leading to a distance resolution of 1.31 cm.

2) Angle-of-Arrival (AoA) Estimation: AoA measurement is another key function in wireless sensing systems. According to the fundamental principles of array signal processing,

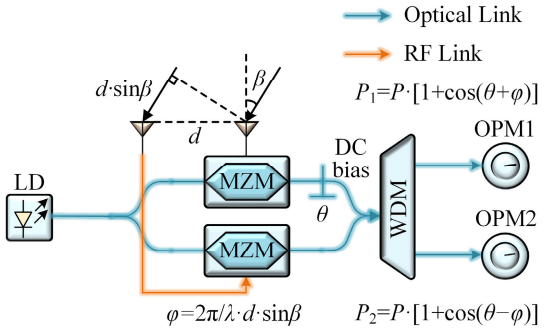

Fig. 6. Microwave photonic AoA estimation system based on optical power measurement. OPM, optical power meter; WDM, wavelength division multiplexer.

AoA estimation can be transformed into a phase detection problem. Assuming that the array interval is d, the relationship between the AoA, denoted by β, and the phase difference between signals received by adjacent antennas, denoted by φ, is expressed as

$$\beta = \arcsin\left(\frac{\varphi \cdot \lambda}{2\pi d}\right) \tag{5}$$

where λ is the wavelength of the received signal. Equation (5) can be derived from the geometric relationship between the two adjacent antennas, as shown in Fig. 6.

Benefitting from ultralow transmission loss, microwave-photonics-based AoA measurement systems can employ larger arrays, thereby enhancing AoA precision. In addition, the ultrawide bandwidth and flexible frequency conversion capabilities of microwave photonic phase detectors enable straightforward AoA estimation [91], [92], [93]. Furthermore, AoA can be mapped to an easily measured parameter, such as optical power [94], [95], [96] or electrical voltage [97], [98], ensuring a fast AoA measurement. For instance, Zhuo et al. [94] introduced a broadband AoA measurement system based on optical power measurement. In this system, RF signals received by two antennas are modulated onto different arms of a dual-parallel Mach–Zehnder modulator (DPMZM), as illustrated in Fig. 6. The +1st and −1st sidebands introduce opposite phase shifts due to the AoA. By adjusting the dc bias of the DPMZM, a phase offset can be introduced into the upper arm signal. After homodyne detection of the two sidebands, respectively, an AoA measurement range of 165° with an error of less than 1.12° was achieved by analyzing the power ratio between the two sidebands. Based on the above basic principle, several improved schemes have been proposed. Chen and Chan [98] utilized optical polarization division to separate the +1st and −1st sidebands in [94] the AOA of microwave signals to the ratio of two dc voltages, which achieves achieving frequency- and power-independent AoA measurement within a range of 0°–63°. The measurement error was less than 2°. We also proposed an omnidirectional AoA measurement scheme using a dual-polarization optical hybrid [93]. By introducing an optical LO signal, a 2-D AoA estimation can be achieved in a single measurement. The measurement error for the elevation angle within the range of −48.08° to 56.43° was better than ±1.63°, and the azimuth angle error within the range of −68.35° to 64.65° was less than ±3.09°.

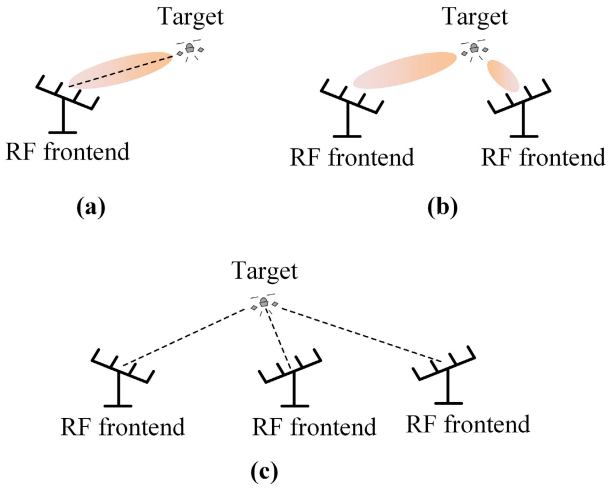

Fig. 7. Three typical microwave photonic positioning architectures. (a) Single-station AoA + ToA. (b) Multistation AoA. (c) Multistation ToA + TDoA. ToA, time of arrival; TDoA, time difference of arrival.

3) Positioning: An RF frontend equipped with an array antenna can perform straightforward positioning using the acquired ranging [or time of arrival (TOA)] and AoA results, as shown in Fig. 7(a). By enabling simultaneous sensing with multiple distributed RF frontends, additional spatial constraints can be introduced, thereby further enhancing positioning accuracy, as illustrated in Fig. 7(b) and (c). Leveraging the low transmission loss inherent in microwave photonics, large-scale distributed RF frontends can be efficiently deployed, with sensing signals centrally processed to achieve high-precision positioning. Yao et al. [99] presented a distributed localization system that achieved high-precision localization with an error of less than 17 cm. The system features a centralized structure consisting of a central unit and multiple detection stations. The positioning signal is distributed across different laser wavelengths. Fu et al. [100] introduce a distributed localization system utilizing fiber-distributed UWB signals, achieving a maximum experimental error of 1.37 cm. Sun et al. [101] present a distributed MIMO radar system based on a bidirectional fiber ring network capable of simultaneously measuring target speed and position. The system achieves localization and speed errors of less than 8 cm and 0.2 m/s, respectively. Benefiting from the flexibility of the bidirectional ring network, the radar can easily extend its nodes and scale up to accommodate a larger operational area. Ma et al. [102] proposed a distributed localization system based on optical recirculating frequency shifting, which can generate stepped frequency signals with bandwidths up to 18 GHz, achieving TOA estimation errors of less than ±5 ps. In addition, the detection of multiple targets at different locations was conducted, with a maximum measurement error not exceeding 1 cm.

4) Imaging: The wireless-based imaging process can be divided into two steps, distinguishing different targets in the distance and azimuth dimension. As discussed above, microwave photonic ranging systems can rapidly distinguish multiple targets in distance with high resolution.

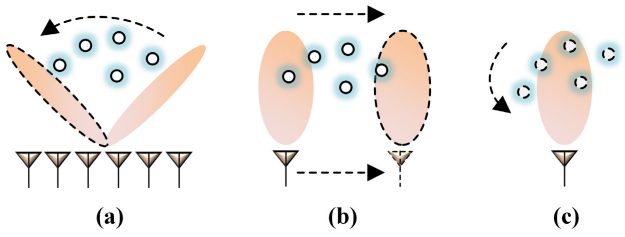

Fig. 8. Three typical microwave photonic imaging methods. (a) Forward-looking imaging. (b) SAR imaging. (c) ISAR imaging. SAR, synthetic aperture radar, ISAR, inverse synthetic aperture radar.

The azimuth resolution is approximately λ/D, where D represents the array's equivalent aperture. Therefore, the most direct approach to improving azimuth resolution is to increase the array antenna size. This is referred to as the forward-looking imaging mode, as illustrated in Fig. 8(a). If the scattering characteristic of the targets remains unchanged, a large array antenna can be equivalently realized by moving the antenna or the targets, as shown in Fig. 8(b) and (c). Numerous microwave photonic technologies have already been applied to high-resolution imaging, including microwave photonic frequency multiplication [89], [103], optical digital-to-analog converters (DACs) [104], frequency-domain mode-locked optoelectronic oscillators (FDML-OEOs) [105], optical recirculating frequency shifting [106], [107], and photonic dechirp-receiving [108]. Among them, signals generated through optical recirculating frequency shifting exhibit the largest bandwidth, which can be applied to achieve the highest imaging resolution, to the subcentimeter or even millimeter level. In addition, recent studies have explored 3-D imaging techniques [109], [110]. For instance, Dong et al. [111] presented an MIMO radar system for 3-D imaging which was designed to capture the geometric features of targets. The system's capability of 3-D imaging is achieved by fusing multichannel 2-D inverse synthetic aperture radar (ISAR) imaging.

5) Spectrum Sensing: In 6G networks, the electromagnetic environment will become increasingly complex, making wireless systems more susceptible to external EMI. To accurately detect targets in such conditions, sensing systems must also be capable of identifying nearby radiation sources in their surroundings. Microwave photonic spectrum sensing systems facilitate wideband, real-time spectrum detection, addressing issues found in traditional electronic technologies, such as limited frequency range, slow processing speeds, and sensitivity to EMI [112].

Microwave photonic spectrum sensing can be broadly categorized into frequency-to-space mapping and frequency-to-time mapping methods, with their fundamental implementation principles illustrated in Fig. 9. In the frequency-to-space mapping approach, the RF signal under test is first mapped into the optical domain. By leveraging abundant spectral resources, such as optical frequency combs (OFCs), the RF spectrum is segmented into smaller portions, facilitating subsequent reconstruction of the RF spectrum using low-speed receivers. In the frequency-to-time mapping approach, the RF signal under test is modulated onto a chirped optical pulse. The modulated RF signal exhibits time-varying carrier frequency characteristics.

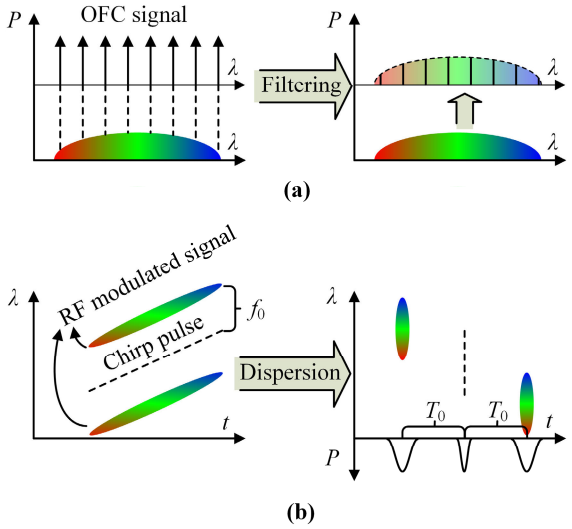

Fig. 9. Two typical microwave photonic spectrum sensing methods. (a) Frequency-to-space mapping. (b) Frequency-to-time mapping. OFC, optical frequency comb.

By passing this optical signal through a carefully designed dispersive medium, the frequency features of the RF signal are translated into temporal features of the optical pulse. Based on the above principles, microwave photonic spectrum sensing can map the frequency to easily measurable parameters like power [113], space [114], phase [115], and time [116], [117]. In addition, photonics-assisted compressed sensing techniques allow for direct spectrum sensing with a sub-Nyquist sampling rate.

6) Multifunction RF System: By integrating active and passive sensing techniques, a multifunction RF system can be achieved, enhancing system reliability. In 2023, we proposed a multifunction scheme for simultaneously measuring frequency and AoA based on frequency–time mapping and angle-power mapping [118]. The angle measurement error was better than $\pm 2.5°$ across a range of $-70°$ to $70°$, and the frequency error was less than ± 12 MHz between 5 and 15 GHz. In 2020, we introduced a system based on the synthetic aperture principle for simultaneous measurement of multitargets' AoAs and frequencies [119]. In addition, we developed a cognitive radio system utilizing microwave photonics [120], [121] to avoid spectrum collision, which integrates spectrum sensing and high-resolution imaging.

7) Other Research: Researchers have also conducted field trials of microwave photonic sensing systems. Bogoni et al. proposed a distributed coherent MIMO radar that maximizes target information extraction through centralized data fusion processing [122], [123], [124]. To provide early warning detection, this radar operates in conjunction with the MONICA standard platform and has been tested at the port of Leghorn in Italy. Zhang et al. [125] introduced a contactless radar for vital sign sensing, operating at a bandwidth of up to 30 GHz, achieving millimeter-level range resolution capable of accurately detecting human behaviors such as breathing. In addition, Li et al. [126] focused on target identification using a high-resolution microwave photonic radar. This approach shows promise for emerging applications in

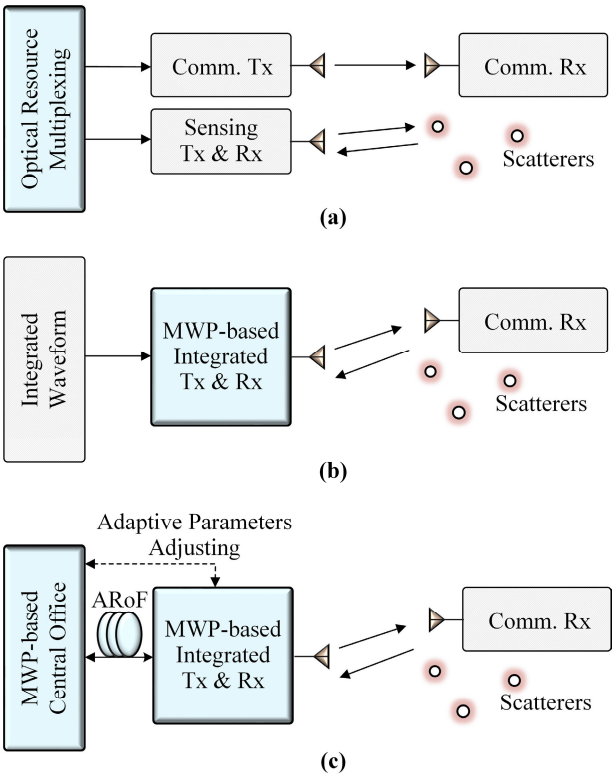

Fig. 10. Three research directions of microwave photonic ISAC technologies. Comm., communication; Tx, transmitter; Rx, receiver. (a) Resource multiplexing. (b) Integrated waveform. (c) Microwave photonic adaptive ISAC base station.

fields such as air defense, security screening, and intelligent transportation.

III. Microwave Photonic ISAC Technologies

Microwave photonic ISAC technologies can be classified into three research directions, as shown in Fig. 10. The first direction involves realizing communication and sensing through resource multiplexing in the optical domain, thereby enhancing the performance of both communication and sensing systems. The second direction focuses on achieving integrated ISAC waveforms based on microwave photonics, which further improves spectral efficiency and simplifies system architecture. The third direction aims to construct microwave photonic ISAC base stations, enhancing overall system performance by jointly utilizing sensing and communication. In this section, we first introduce typical microwave photonic ISAC frontend transceiver architectures. Then, the recent research about the aforementioned three directions is overviewed.

A. Microwave Photonic ISAC Frontend Transceiver

Fig. 11(a) shows a typical microwave photonic ISAC frontend transceiver architecture. Most microwave photonic ISAC systems in the literature are built based on this architecture or its enhanced variants. In the transmitter, the baseband or low-frequency ISAC signals are frequency-converted or multiplicated into the corresponding RF signal bands. The signals for sensing are reflected by surrounding scatterers, and then the ISAC receiver down-converts or preprocesses the reflected signals in the optical domain. An ADC samples the baseband or intermediate frequency (IF) signal to extract the corresponding sensing results.

In the microwave photonic transmitter, optical heterodyne, OFC-based up-conversion, or photonic frequency-multiplication techniques are usually applied, as shown in Fig. 11(b). The optical heterodyne method [127], [128] generates RF signals by beating two laser wavelengths in a PD, allowing for the direct up-conversion of baseband signals from a DAC. In Fig. 11(b1), two single-wavelength lasers are chosen as the two wavelengths. However, the relative frequency shift and phase noise of the laser wavelengths affect the generated RF signal, necessitating a series of digital signal processing steps in the receiver. These include clock recovery, carrier recovery, and differential decoding for communication, as well as frequency offset and phase noise compensation for sensing. The two specific wavelengths can also be selected from an OFC [129], [130] using a wavelength division multiplexer, as depicted in Fig. 11(b2). Considering that the frequency repetition of the OFC can be locked to a stable atomic clock, it is possible to suppress additional frequency noise arising from optical-to-electrical conversion. In Fig. 11(b3), the photonic frequency-multiplication method [131], [132] relies on the nonlinear effects of optoelectronic devices under large signal modulation, driven by an electronic IF signal. This produces multiple equidistant sidebands in the optical spectrum. An optical filter then selectively removes the optical carrier and other unnecessary sidebands, enabling the beating of specific high-order sidebands in a PD. The frequency stability of the generated RF signal is mainly determined by the performance of the electronic IF signal. However, this method distributes optical power among multiple subcarriers, resulting in a significant reduction in the SNR.

Microwave photonic receiver architectures can be classified into three main types: electrical down-conversion, photonic RF down-conversion, and photonic dechirping, as illustrated in Fig. 11(c). In Fig. 11(c1), the received RF signal is down-converted using an electronic mixer and then transmitted to the ADC through an RoF link. If the ADC is located near the receiving antenna, the down-converted signal can be directly transmitted via an electrical cable. Alternatively, as shown in Fig. 11(c2), down-conversion can be achieved in a photonic-based mixer, where the LO signal and the received RF signal are both modulated on a dual-drive MZM. The electronic down-converted signal can be obtained through optical-to-electrical conversion. Photonic RF down-conversion [133], [134] is noted for its wide flat response bandwidth and high port-to-port isolation, offering advantages over traditional electronic mixer. In recent years, photonic RF down-conversion has gain significant attention in RoF communications [135], satellite payloads [136], [137], ISAC systems [138], and radar systems [139], [140]. Photonic dechirping [141], [142], primarily applied for LFM signal demodulation, is another interesting technique in ISAC systems. Its principle is illustrated in Fig. 11(c3). It is a specialized form of photonic RF down-conversion where the LO signal is replaced by an LFM signal. The frequencies of the output signal from

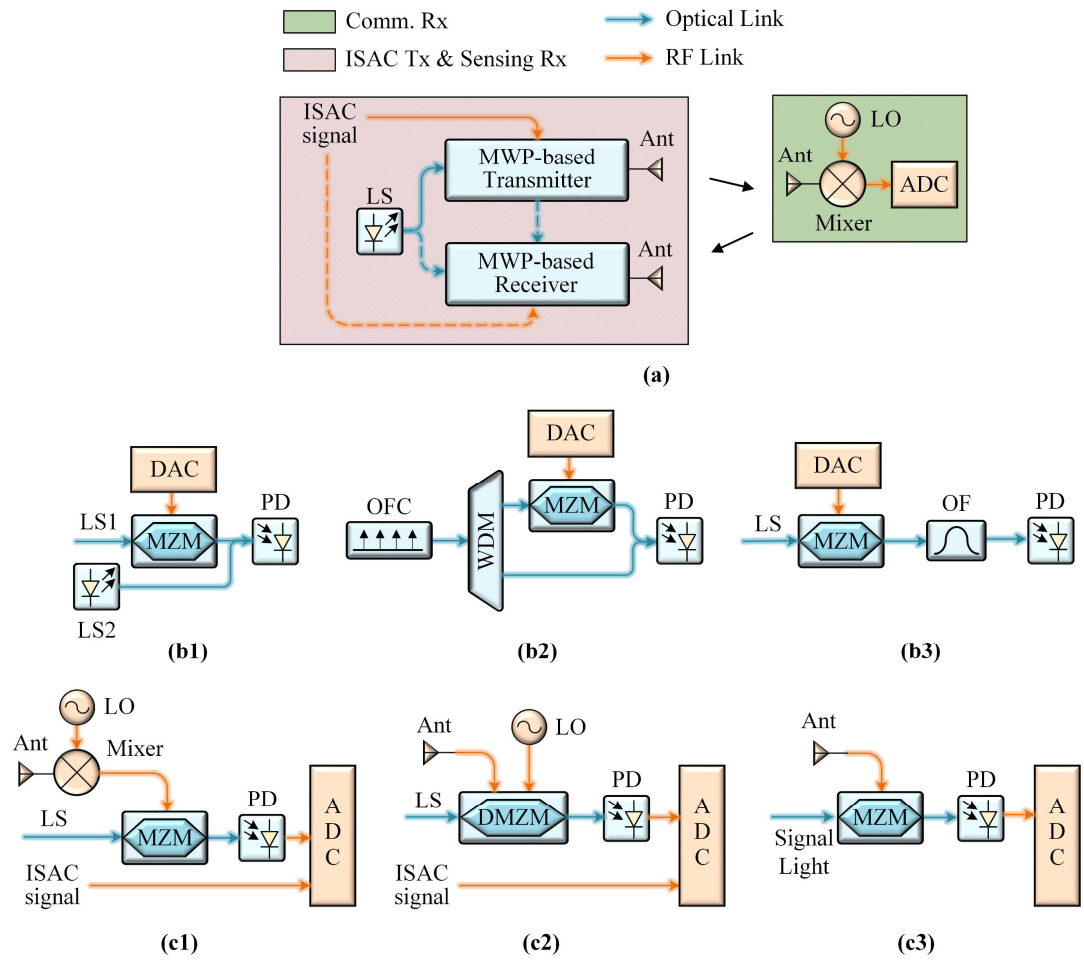

Fig. 11. (a) Schematic of a typical microwave photonic ISAC frontend transceiver. (b) Three typical microwave photonic transmitter architectures: optical heterodyne, OFC-based up-conversion, and photonic frequency multiplication. (c) Three typical microwave photonic receiver architectures: electrical down-conversion, photonic down-conversion, and photonic dechirping. DMZM, dual-drive MZM; OF, optical filter.

the PD are proportional to the distance of the scatterers. In this architecture, the pulse compression process is achieved in the analog domain [87], [88], avoiding using broadband analog-digital conversion and large data volume digital signal processing. To achieve optimized performance using minimized hardware resources, the choice of microwave photonic ISAC frontend architecture should take into account the specific application scenarios and performance requirements.

B. Resource Multiplexing

One key advantage of microwave photonics over traditional electronic technologies is its capability to access additional optical resources. In the previous section, we briefly introduced how PDM and WDM can facilitate the generation of high-capacity wireless communication signals. Furthermore, the relatively flat broadband characteristics and fast tuning capabilities of optical devices enhance the implementation of traditional techniques such as TDM and FDM. Table II summarizes representative microwave photonic ISAC research based on resource multiplexing. In this subsection, we review the current research status of these studies in detail, highlighting key findings and advancements in the field.

1) Traditional Resource Multiplexing: Time and frequency are the typical orthogonal dimensions widely used in traditional radar, communication, and MIMO systems. In ISAC, utilizing these resources allows for the separation of communication and sensing functions, thereby reducing EMI. Given the advancements in digital signal processing, TDM has emerged as the most mature solution for ISAC. TDM transmits communication and sensing signals at different times, naturally achieving interference separation. Wang et al. generated TDM ISAC signals using optical heterodyne [143] and photonic frequency multiplication [144], achieving signal bandwidths in the tens of gigahertz, leading to a range resolution of 1 cm for sensing and a data rate of 46.55 Gbit/s for communication. Fang et al. [145] developed a silicon-based integrated ISAC transceiver chip, realizing a range resolution of 4.94 cm and a communication rate of 36 Gbit/s in TDM mode.

Although TDM is a relatively mature technology, it requires time-domain segmentation of ISAC signals, which can affect real-time communication and reduce sensing accuracy. In contrast, FDM allows communication and sensing to operate simultaneously within any time period, offering greater flexibility in signal design and application. While FDM necessitates additional hardware for selecting separate frequency bands, its advantage lies in the inherent wideband capabilities of microwave photonics, making it more attractive for ISAC applications. For instance, Lei et al. [147] presented a system

TABLE II
REPRESENTATIVE STUDIES OF MICROWAVE PHOTONIC ISAC SYSTEMS BASED ON RESOURCE MULTIPLEXING

Multiplexing technique	Signal generation method	Center frequency (GHz)	Total bandwidth (GHz)	Data rate (Gbit/s)	Sensing resolution (cm)	Spectral efficiency (bit/s/Hz)	Ref
TDM	Optical heterodyne	77	15	46.55	1.02	3.10 (64QAM)	[143]
	Frequency-multiplication	92	20	10	0.94	0.5 (QPSK)	[144]
	OFC-based up-conversion	28	10	36	4.94	3.6 (64QAM)	[145]
	Optical heterodyne	340	10	38.1	1.58	3.81 (MQAM)	[146]
FDM	Frequency-multiplication	16/25.4	4.37	2.3	4.66	0.53 (BPSK)	[147]
	Optical heterodyne	100	1.78	3.125	8.3	1.76 (QPSK)	[148]
	Optical heterodyne	100	1.8	3.2	8.3	1.78 (16QAM)	[149]
	Optical heterodyne	84.5/94.5	12.5	78	3	6.24 (MQAM)	[150]
	OFC-based up-conversion	60	6.5	18	0.97	2.77 (16QAM)	[151]
PDM	Optical heterodyne	124/151	47.66	251.03	2.5	5.27 (16QAM)	[152]
	OFC-based up-conversion	28	4.02	23	30	5.72 (16QAM)	[153]
WDM	OFC-based up-conversion	2.475/4.9	0.02	0.054	750	2.7 (64QAM)	[154]
	OFC-based up-conversion	370	28.5	56	1.1	1.96 (16QAM)	[155]
	OFC-based up-conversion	275	30	120	0.25	4 (32QAM)	[156]

utilizing a dual-drive MZM to generate low-frequency binary phase shift keying (BPSK) communication signals alongside photonic frequency-multiplication LFM signals, achieving a data rate of 2.3 Gbit/s and a range resolution of 4.66 cm. However, the utilization of lower-order modulation typically limits spectral efficiency, as fewer bits are transmitted per symbol. If the EVM is sufficiently low, the system's spectral efficiency can be enhanced by employing higher-order modulation techniques.

Liang et al. [149] explored the generation of FDM-ISAC signals via the optical heterodyne method with geometrically shaped (GS) 16-QAM modulation. To improve the symbol error rate with high-order modulation, an artificial intelligence (AI) network was applied, achieving a 0.5-dB improvement in receiver sensitivity. A data rate of 3.2 Gbit/s and a range resolution of 8.3 cm was achieved. In addition, Wang et al. [150] constructed an ISAC system based on FDM in the W band that leverages M-ary QAM modulation to attain data transmission rates of up to 78 Gbit/s with a radar resolution of 3 cm. Furthermore, Song and He [148] proposed a system integrating LFM and OFDM signals for ISAC, utilizing nonorthogonal multiple access (NOMA) techniques to improve spectral efficiency by enabling multiuser communication, achieving an equivalent data rate of 3.125 Gbit/s and a range resolution of 8.3 cm.

Nonetheless, FDM inherently suffers from lower spectral efficiency because both communication and sensing share parts of the spectrum. To address this issue, Zhong et al. [151] introduced a novel microwave photonic millimeter-wave ISAC system utilizing a coherent fusion process (CFP) of sparse sub-band LFM signals. This approach achieved full-band equivalent range resolution within a small portion of the total bandwidth, while allocating more spectral resources to communication, thereby significantly enhancing the spectral efficiency of the ISAC system. Using 16-QAM modulation, the system achieved an impressive data rate of 18 Gbit/s and a range resolution of 0.97 cm with only 6.5 GHz of bandwidth, representing one of the highest comprehensive performances in microwave photonic ISAC systems based on FDM.

2) Optical Resource Multiplexing: Microwave photonics can leverage additional optical resources via multiplexing techniques like PDM and WDM. For instance, Lei et al. [152] discussed a 2 × 2 MIMO system constructed by multiplexing two optical orthogonal polarization states, while communication and sensing functions are separated via FDM. The architecture achieves a real-time data rate of 251.03 Gbit/s and a range resolution of 2.5 cm, with a spectral efficiency of 5.27 bit/s/Hz under 16-QAM modulation. In [153], communication and sensing functions were assigned to different polarization states of an optical signal, as shown in Fig. 12. The upper branch utilized an MZM for carrier-suppressed double-sideband generation, producing two LO optical signals, and the lower branch employed an I/Q modulator for single-sideband modulation, converting both LFM and 16-QAM signals into the optical domain. The two wavelength division multiplexers regrouped the ISAC signals and LO signals into two channels, which were polarization multiplexed. By using a polarization-insensitive optical bandpass filter to select the required LO signal, the communication and sensing can be separated before photodetection. This system enables centimeter-level ranging accuracy in the Ku band and a wireless data rate of 23 Gbit/s at 28 GHz, with a spectral efficiency of 5.72 bit/s/Hz.

PDM can also facilitate additional functionalities. Men et al. [157] employed a dual-polarization BPSK (DP-BPSK) modulator for signal generation. In this setup, communication and sensing signals are up-converted and modulated onto different polarization states through the upper and lower arms of the DP-BPSK modulator, respectively. By adjusting the polarization state of the optical signal before it passes through the polarizer, the power ratio between communication and sensing signals can be dynamically controlled, allowing for flexible switching between functions. Ge et al. [158] utilized PDM to enable multitarget detection and Doppler decoupling in ISAC systems.

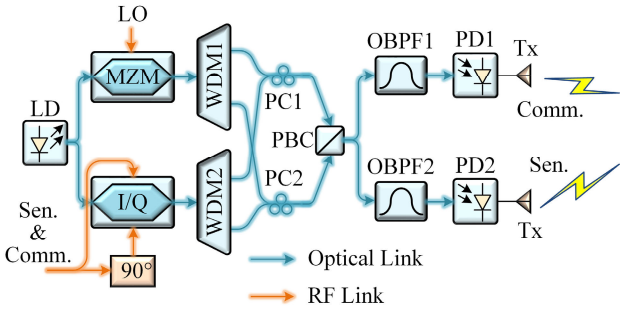

Fig. 12. Schematic of a microwave photonic ISAC system based on PDM. I/Q, in-phase/quadrature; POF, programmable optical filter; PC, polarization controller; PBC, polarization beam combiner; OBPF, optical bandpass filter.

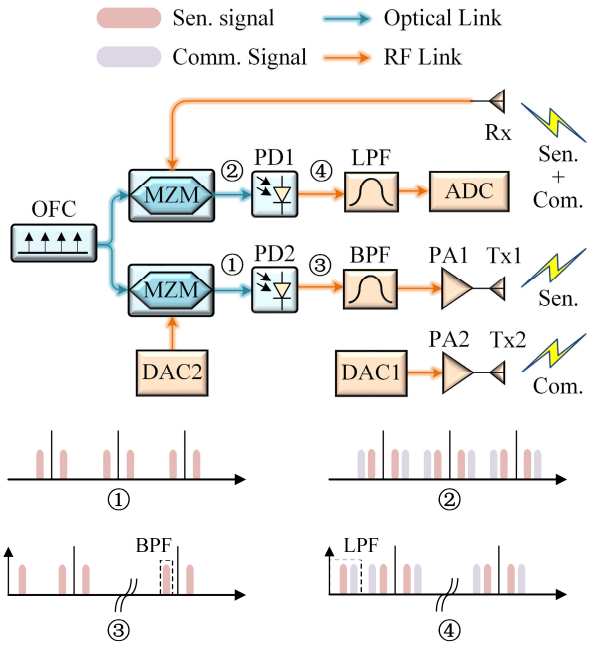

Fig. 13. Schematic of a microwave photonic ISAC system based on WDM.

WDM can fully utilize the rich wavelength resources in the optical domain. OFCs, consisting of a series of evenly spaced and coherent frequency components, can greatly enhance the capabilities of microwave photonics together with WDM. In [154], an OFC-based ISAC system was proposed, and its schematic is shown in Fig. 13. In this system, the sensing signals are upconverted by an OFC generated from a mode-locked laser (MLL). An electrical bandpass filter then selects the sensing signal within a specific frequency band. Upon reception, ISAC signals are down-converted by beating the modulated signal with the nearest frequency component of OFC in the optical domain. Finally, a low-speed receiver extracts and processes the sensing and communication information. This system achieved a data rate of 54 Mbit/s and a range resolution of 7.5 m. In addition, the OFC can be regarded as a series of narrow pulses, each containing abundant frequency components in the time domain. In [155], the optical pulses generated by an MLL passed through a highly dispersive medium. Due to the dispersion effect, the frequency components within each optical pulse were gradually separated, ultimately forming an optical LFM signal. By beating this optical LFM signal with a single-frequency optical signal, a 330-GHz carrier frequency LFM with a bandwidth of 21 GHz was generated. This ISAC system achieved a data rate of 56 Gbit/s and a range resolution of 1.1 m. However, the frequency repetition of MLL-based OFC is generally limited, which restricts the frequency selection flexibility in ISAC system design. An OFC generated by electrooptic modulation offers more adaptability in repetition rate selection. Lyu et al. [156] used phase modulation to generate an OFC with a 25-GHz spacing. Three comb lines at 250, 275, and 300 GHz were selected using a programmable optical filter as carriers for generating ISAC signals. The transmitter scheme is similar to that depicted in Fig. 11(b2). To enhance the communication spectrum efficiency and sensing resolution, they proposed a multichannel coherent fusion algorithm using autoregression to fully utilize the three sub-bands and the intervening spectral gaps, achieving an impressive range resolution of 0.25 cm and a data rate of up to 120 Gbit/s.

C. Integrated Waveform

ISAC technologies based on multiplexing techniques require resource partitioning and scheduling while minimizing interference between communication and sensing functions. In practical applications, however, the available spectrum resources and the hardware redundancy for sensing and communication are often limited. To address this challenge, a technique called integrated waveform has emerged. This method enables a single set of signal waveforms to simultaneously realize communication and sensing functions. By eliminating the need for separate generation and processing of communication and sensing signals, this method promotes better integration of frontend design and baseband signal processing.

From a mathematical perspective, designing an integrated waveform involves solving a multiconstraint optimization problem. The waveform must balance the performance requirements of communication and sensing across various application scenarios. Moreover, it is crucial to ensure that the shared waveform avoids potential interference between communication and sensing functions. Currently, integrated waveform technologies in microwave photonics are primarily categorized into two groups: those based on OFDM and those based on LFM. In addition, spread spectrum modulation techniques can be employed to achieve ISAC in complex interference environments.

1) Orthogonal Frequency Division Multiplexing (OFDM): The 4G and 5G wireless communication systems have widely adopted OFDM waveforms. Leveraging OFDM signals for sensing functions can avoid large-scale modifications to existing communication architectures, facilitating a smooth transition from 5G to 6G while minimizing changes to the current network infrastructure [159]. The baseband OFDM signal can be mathematically expressed as

$$s_{\mathrm{OFDM}}(t)=\sum_{m=0}^{N_s}\left[\mathrm{rect}\left(\frac{t-mT_s}{T_s}\right)\sum_{n=0}^{N_c}d_{m,n}e^{j2\pi n\Delta f t}\right] \quad (6)$$

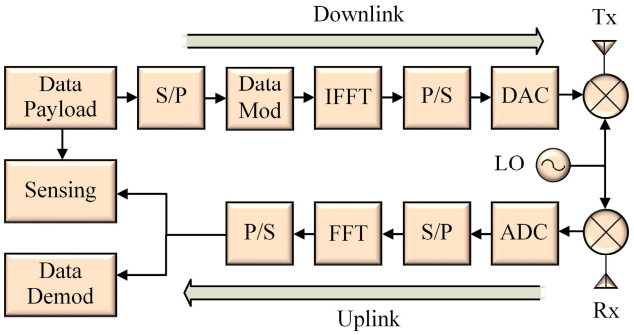

Fig. 14. Signal processing flowchart of OFDM-based ISAC system. Demod, demodulation; S/P, serial to parallel; P/S, parallel to serial; FFT, fast Fourier transform; IFFT, inverse FFT.

where N_s and N_c are the number of OFDM symbols and subcarriers, $d_{m,n}$ is the data symbol transmitted on the nth subcarrier during the mth OFDM symbol, Δf is the subcarrier spacing, T_s is the OFDM symbol duration, and rect(...) is a rectangular pulse function. The signal processing flowchart of an OFDM-based wireless ISAC system is presented in Fig. 14. After wireless transmission, each OFDM subcarrier experiences magnitude loss and phase shifts induced by the environment and surrounding scatterers. The OFDM signal can be regarded as performing a frequency-domain discrete sampling based on its subcarrier. By applying the Fourier transform to the subcarriers and symbols, the delay and the Doppler frequency of the target can be estimated.

To date, the application of OFDM-based ISAC systems encounters three key challenges. First, the use of multiple subcarriers for parallel transmission results in a high PAPR, which can exacerbate nonlinear distortions in microwave photonic links. Second, OFDM is highly sensitive to phase noise, carrier frequency offset, and Doppler frequency shifts. In millimeter-wave and terahertz bands, current signal generation methods such as optical heterodyne or electronic frequency multiplication, can worsen phase noise, thereby degrading ISAC system performance. Lastly, OFDM is designed primarily for communication systems, which tends to have a low peak sidelobe ratio (PSLR) in its autocorrelation function, resulting in a poor sensing performance for multitargets detection.

Extensive research has been conducted to address these issues. Umezawa et al. [176] first validated a wireless sensing system using OFDM in the millimeter-waveband. Huang et al. [160] proposed a microwave photonic ISAC architecture based on an ARoF link, which generated up-converted OFDM signals through double-sideband suppressed-carrier modulation. This setup employed the partial sequence segmentation (PTS) technique to reduce PAPR, ultimately achieving multitarget detection capability with a range resolution of 30 cm. The communication rate reached 1.56 Gbit/s. Peng et al. [161] utilized optical heterodyne methods for up-conversion and introduced decision feedback frequency-domain Volterra nonlinear equalization (DF-FD-VNLE) technique to compensate for nonlinear distortions, improving the sensitivity of the OFDM receiver by 1.8 dB. In addition, by incorporating a multiple signal classification (MUSIC) algorithm, commonly used in radar, into the OFDM system, the PSLR was improved by 18.6 dB.

In terms of phase noise issues, Xue et al. [138] analyzed its impact on the performance of OFDM-based ISAC systems and introduced an optoelectronic oscillator (OEO) to produce low phase noise OFDM signals. Benefiting from the low transmission loss of optical fiber, OEOs [177], [178], [179] can incorporate kilometers of fiber into their cavity, which significantly improves the quality factor of the oscillator. The phase noise of a 10-GHz microwave signal can reach −163 dBc/Hz at 6-kHz frequency offset [180]. In [138], a low phase noise OFDM-based ISAC system was realized by employing an OEO. The integration of the OEO significantly improved the EVM from 12.5% to 4.7%, facilitating the use of higher-order modulation to boost the data rate. The system achieved a range resolution of 1.5 cm and a data rate of 32 Gbit/s within the 90-GHz band. In addition, to simplify the hardware architecture, Liu et al. [162] proposed a virtual-carrier-aided self-coherent (VCA-SC) OFDM technique that eliminates the effects of phase noise using a digital LO. However, this method introduces self-interference during envelope detection at the receiver end, necessitating the use of a Kramers–Kronig receiver for interference cancellation. This scheme achieved a data rate of 16 Gbit/s and a range resolution of 4.8 cm. Recent research on OFDM-based ISAC systems [163], [164] has explored additional phase noise suppression methods, such as principal component phase equalization and blind phase search (PCPE-BPS). These studies demonstrated a spectral efficiency of 3 bit/s/Hz and a range resolution of less than 1 cm using 16-QAM modulation. These results surpass the best performance metrics previously observed in FDM-based ISAC systems [151].

2) Linear Frequency Modulated (LFM) Signal: LFM signals, which have been widely applied in microwave photonic radars [181], leverage the benefits of large time-bandwidth product and photonic dechirping. Compared to OFDM signals, LFM signals generally have a constant envelope and relatively low peak power, which would introduce lower nonlinearity in microwave photonic links. The LFM signal can be mathematically written as

$$s_{\mathrm{LFM}}(t) = A \cdot \mathrm{rect}\left(\frac{t - T_s}{T_s}\right) \exp\left(j2\pi f_c t + \pi k t^2 + \phi\right) \quad (7)$$

where k is the chirp rate. To achieve an integrated waveform based on LFM for ISAC, communication information should be encoded into the amplitude, phase, or frequency of the LFM signal, denoted as A, ϕ, and f_c in (7). The time–frequency characteristics of LFM-based integrated waveforms are illustrated in Fig. 15. Generally, this integration results in degraded sensing performance, as the randomness of communication data can disrupt the excellent autocorrelation properties of the LFM signal.

Our team [165] has successfully embedded amplitude-shift keying (ASK) signals into LFM signals to achieve microwave photonic ISAC. Using photonic frequency-multiplication modulation, we generated an LFM-ASK signal with an 8-GHz bandwidth, achieving real-time imaging with a resolution of 2 cm and a data rate of 100 Mbit/s. However, incorporating

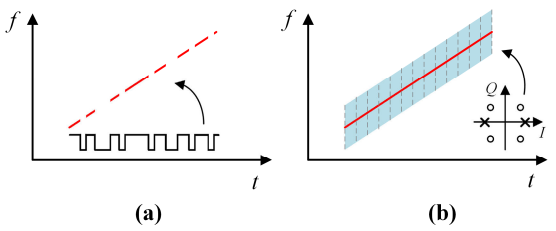

Fig. 15. Time–frequency characteristics of LFM-based integrated waveforms. (a) LFM-ASK waveform. (b) LFM-BPSK and LFM-QPSK waveform.

ASK signals significantly deteriorates the PSLR of the LFM signal, reducing it to just 9.5 dB. In subsequent research, Lyu et al. [166] demonstrated that embedding PSK signals into LFM signals can substantially enhance the PSLR to 20.9 dB. They verified a data rate of 6 Gbit/s and a range resolution of 1.3 cm.

To improve the communication rate of LFM-based ISAC systems, researchers have further explored high-order modulation schemes and large bandwidth spectrum utilization. This approach increases the demand for signal synchronization due to the continuous frequency changes over time in LFM signals, in contrast to OFDM signals where subcarriers maintain fixed frequencies within a timeframe [182]. Addressing this challenge, Lei et al. [168] proposed a method that used pulse compression to achieve signal synchronization in LFM-based ISAC systems. This method validated an LFM-QPSK waveform that achieved a data rate of 11.5 Gbit/s and a PSLR of 16.5 dB. Lyu et al. [169] observed that increasing the symbol rate can mitigate the negative effects of QPSK modulation on the autocorrelation characteristics of LFM, as the communication signal behaves more like a random signal. This results in a theoretical approximation of orthogonality with increased symbol bits in the autocorrelation. They introduced a dual-chirp LFM signal for synchronization, which significantly reduced the power overhead from 8.3% to 0.5%. This enhancement successfully increased the data rate to 20 Gbit/s and achieved a PSLR of 29.2 dB. Furthermore, the dual-chirp LFM signal allows for adaptive frequency compensation through fractional Fourier transforms [183], with estimation errors below 0.08%.

In addition, related research has explored combining OFDM and LFM signals in ISAC systems. OFDM offers robustness against frequency fading and multipath interference, facilitating higher-order modulation schemes. The utilization of subcarriers effectively reduces the symbol rate, which in turn lowers the demand for signal synchronization. Bai et al. [170] proposed a constant envelope (CE) OFDM technique in an LFM-based ISAC system to reduce the nonlinear effects introduced by microwave photonic links. Bai et al. [171] employed an OFC to generate LFM-OFDM signals with multiple frequency bands. This approach achieved enhanced range resolution, achieving a data rate of 16 Gbit/s and a range resolution of 0.86 cm.

As detailed in Table III, ISAC schemes based on LFM waveforms currently exhibit lower spectral efficiency compared to those based on OFDM waveforms. However, within microwave photonic systems, LFM waveforms offer photonic

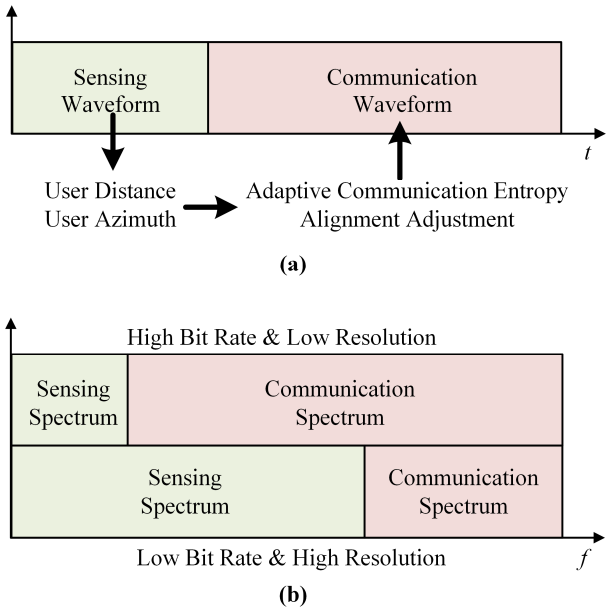

Fig. 16. Parameter adjustment in ISAC system. (a) TDM mode. (b) FDM mode.

dechirping, flexible signal generation, and superior multitarget detection capabilities. In future 6G ISAC applications, LFM-based integrated waveforms are expected to play a significant role.

3) Spread Spectrum Signal: Spread spectrum technology spreads the signal over a large frequency band, which can enhance resistance to interference and help protect user privacy in specific scenarios. Bai et al. [173] proposed a microwave photonic spread spectrum technique based on phase encoding, utilizing cascaded intensity modulation and polarization modulation. This approach generates wideband millimeter-wave ISAC signals, achieving a range resolution of better than 3.5 cm and a wireless data rate of over 1 Gbit/s. Xue et al. [174] generated a high-frequency LO signal within an OEO loop, employing I/Q modulation to modulate the ISAC spread spectrum signal onto the optical carrier. The experiments demonstrated a data rate of 335.6 Mbps, a range resolution of 7.5 cm, and a PSLR of 20 dB. Alzamil et al. [175] validated an ISAC system that combines a kilometer-length ARoF link with a spread spectrum technique, ensuring reliable communication and sensing performance. Overall, while the spectral efficiency of ISAC using spread spectrum technology is relatively low, it offers excellent PSLR and enhanced resistance to interference, making it promising for practical applications in scenarios such as V2X.

D. Microwave Photonic Adaptive ISAC Base Station

The above techniques focus on specific technical aspects within microwave photonic ISAC but do not provide a comprehensive discussion on constructing microwave photonic ISAC base stations. Brandão et al. [184] proposed a microwave photonic CRAN architecture, which utilized ARoF and WDM to transmit 2 × 2 MIMO signals in both uplink and downlink. By incorporating 5G new-radio (NR) waveforms, the system achieved a ranging accuracy of 7 cm and an EVM of less than 15%.

TABLE III
REPRESENTATIVE STUDIES OF MICROWAVE PHOTONIC ISAC SYSTEMS BASED ON INTEGRATED WAVEFORM

Waveform	Modulation method	Total bandwidth (GHz)	Data rate (Gbit/s)	Sensing resolution (cm)	Spectral efficiency (bit/s/Hz)	Technique/Features	Ref
OFDM	16QAM	0.5	1.56	30	3.12	PTS* (PSLR:14.5 dB)	[160]
	16QAM	1	4	10	4	DF-FD-VNLE*; MUSIC**	[161]
	16QAM	2	6.4	7.5	3.2	OEO***	[138]
	16QAM	4	16	4.8	4	VCA-SC***	[162]
	16QAM	16	47.06	0.96	2.94	FDF**; PCPE-BPS***	[163]
	16QAM	16	47.54	0.98	2.97	two-stage CFR***	[164]
LFM	ASK	8	0.1	2	0.08	(PSLR: 9.5 dB)	[165]
	PSK	12	6	1.3	0.5	(PSLR: 20.9 dB)	[166]
	QPSK	1	0.21	3.25	0.21	/	[167]
	QPSK	8	11.5	10.4	1.44	(PSLR: 16.5 dB)	[168]
	QPSK	10	20	1.5	2	Dual-chirp (PSLR: 29.2 dB)	[169]
	16QAM	20	8	1.5	0.8	CE-OFDM (PSLR: 15 dB)	[170]
	16QAM	12	16	0.86	1.3	Multiple band OFDM	[171]
	64QAM	9	6	1.76	0.67	OFDM (PSLR: 15 dB)	[172]
Spread spectrum	BPSK	10	1	3.5	0.1	(PSLR: 12.1 dB)	[173]
	QPSK	2	0.34	7.5	0.17	(PSLR: 20 dB)	[174]
	BPSK	0.7	0.05	43	0.07	(PSLR: 18 dB)	[175]

*Techniques improve PAPR; **Techniques improve PSLR; ***Techniques improve phase noise.
FDF: frequency domain filtering; CFR: carrier frequency recovery.

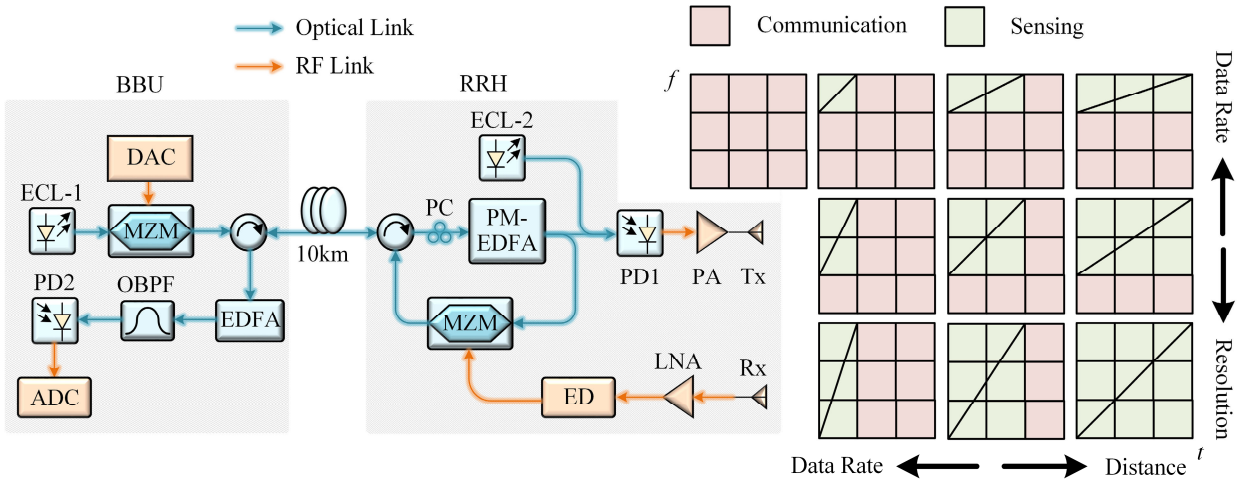

Fig. 17. Schematic of a microwave photonic ISAC base station based on a time–frequency division multiplexed (TFDM) waveform. ECL, external cavity laser; PM-EDFA, polarization-maintaining erbium-doped fiber amplifier; ED, envelope detector.

In practical scenarios, a fixed-parameter ISAC system often falls short in meeting dynamic requirements. Therefore, microwave photonic ISAC base stations need to adaptively adjust parameters to flexibly assign resources to communication and sensing functions [185]. Given that integrated waveforms are still in the exploratory stage and no unified theoretical model currently exists to balance communication and sensing performance, adaptive parameter adjustment through resource multiplexing emerges as a more effective approach for 6G. A typical adaptive parameter adjustment scheme is illustrated in Fig. 16. Jia et al. [186] proposed a W-band microwave photonic ISAC base station with sensing-assisted communication capability operating in the TDM mode. The sensing function first determines the user's distance and position, which enables the system to estimate the communication capacity of the available channel. These results are then used to adjust the beam direction directly, enhancing the data rate to a peak of 68.6 Gbit/s while maintaining the sensing resolution of 2 cm. Meanwhile, Dong et al. [187] proposed a W-band flexible ISAC system with adaptive waveforms operating in the FDM mode, which could dynamically adjust the bandwidth allocated to LFM and OFDM signals. By assigning more bandwidth to the LFM signal, the ranging capability improves while the data rate is reduced. In an experiment, the proposed system achieved a tunable data rate ranging from 5.98 to 41.48 Gbit/s, while the range resolution could be adjusted from 1.53 to 6.94 cm.

To further improve the spectrum efficiency, we proposed a microwave photonic ISAC scheme based on a time–frequency division multiplexed (TFDM) waveform [188], which has been

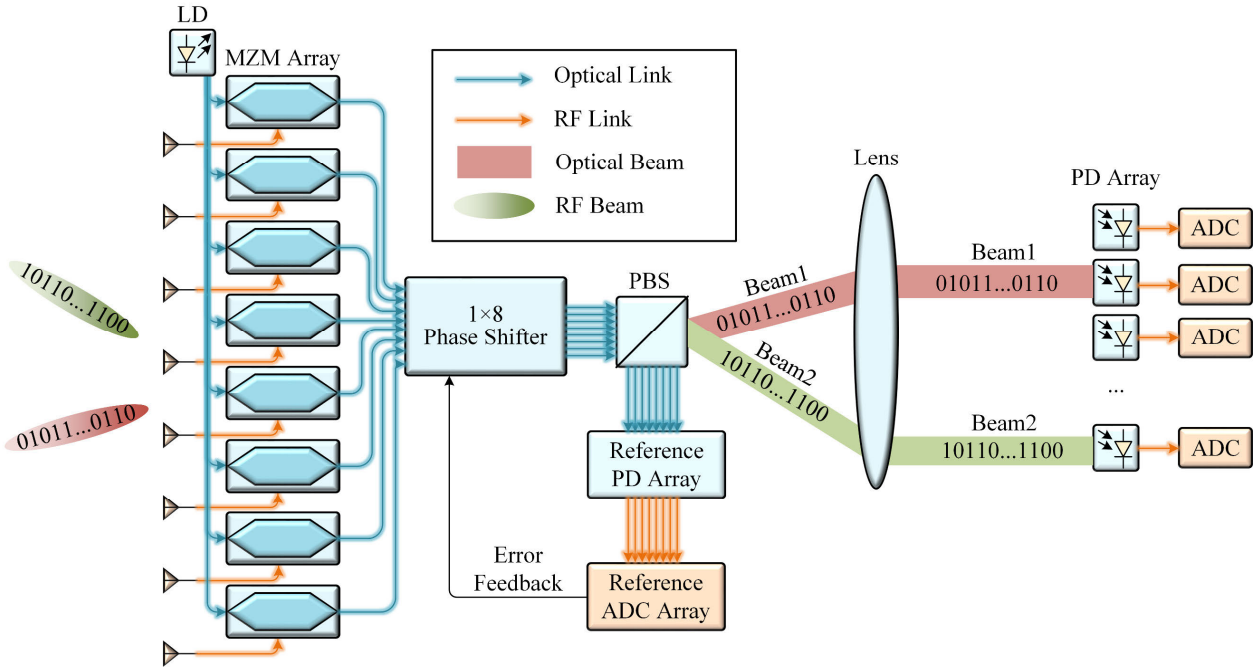

Fig. 18. Schematic of the eight-channel microwave photonic frontend receiver based on holographic radio concept. PBS, polarization beam splitter.

validated within the framework of a microwave photonic base station. The schematic is depicted in Fig. 17. The BBU selects the appropriate TFDM waveform based on the scenario's requirements and transmits the baseband signal over a 10-km RoF link to the RRH. At the RRH, the signal is up-converted to the W-band via optical heterodyne. The received sensing signals are then sent back to the BBU via the RoF link for detection and processing. Unlike traditional TDM and FDM, our approach defines ten distinct signal bandwidth and time width allocation schemes, with the time–frequency characteristics shown in the right part of Fig. 17. These designs allow for flexible switching among high-resolution sensing, large-range detection, and high-speed communication, effectively leveraging time and frequency resources in specific application scenarios. Experiments validated a tunable data rate ranging from 15 to 60 Gbit/s and an adjustable range resolution from 1.53 to 4.39 cm over a 10-km ARoF link.

IV. Discussion and Conclusion

Other microwave photonic technologies are also expected to play an important role in 6G ISAC systems. First, microwave photonics can exploit optical nonlinear characteristics for analog signal processing in the optical domain [189], [190]. This includes using dispersive optical waveguides to achieve real-time Fourier transform [191], [192] or employing optical nonlinear elements to construct artificial neural networks (ANN) [193], [194]. Photonic ADCs [195], [196], known for their ultralow time jitter and high sampling accuracy, are capable of sampling large-bandwidth RF signals using a low sampling rate and low bandwidth electronic ADC. This significantly reduces the receiver demand for multistage frequency conversion and high-performance eletronic ADC. Second, ARoF holds promise for implementing distributed ISAC architectures. Current microwave photonic time–frequency synchronization techniques [197], [198], [199], [200], [201] are expected to support multibase station operations within a cell-free framework. In addition, optically controlled phased arrays [202], [203], [204], based on microwave photonics, can precisely control broadband electromagnetic wave beams, providing spatial dimension resources for ISAC. Moreover, advancements in integrated microwave photonics [205], [206], [207], [208] can lead to the development of low-cost, low-power, and miniaturized base stations.

Holographic radio [209] is another interesting concept anticipated for application in ISAC, which is enabled by microwave photonics. It employs radio holographic and wave field synthesis techniques to manipulate RF beams with high precision. Fig. 18 illustrates a system to realize holographic radio using an eight-channel microwave photonic frontend receiver. The antenna array receives RF signals from the free space and discretely samples the information. Spatial Fourier transforms can be performed using a lens, and the optical intensity is directly detected by a PD array at the lens's focal plane. The directions of the incoming beams are mapped to the positions of the spatial light intensity. To compensate for optical phase shifts introduced by the array fibers, light reflected by the polarization beam splitter (PBS) is mixed with a reference beam from the main laser in another PD array. The beat frequency signals are used to track phase shifts in the eight independent optical fiber paths, enabling phase error detection and adaptive compensation.

Holographic radio enables ultramassive MIMO in a 6G network [210], optimizing the flexibility and accuracy of beamforming. The fine resolution and manipulation of the RF beam provide exceptional beamforming and AoA estimation

capabilities, fulfilling the future 6G communication demands for ultrahigh data rate and ultralow latency. In addition, the accuracy and resolution of existing AoA estimation methods based on array signal processing depend on the size of the array. Using the concept of holographic radio to sense RF beams can address issues related to array size limitations. Notably, holographic radio focuses solely on the characteristics of RF beams and does not require additional signal design to achieve finely controllable beams. This simplicity provides robust technical support for the implementation of ISAC in 6G wireless networks [211].

This article provides an overview of the research status of microwave photonic ISAC technologies, focusing on microwave photonic ISAC frontend transceivers, resource multiplexing, integrated waveform design, and adaptive parameter adjustment. Currently, resource multiplexing in ISAC is relatively mature, with microwave photonics effectively and flexibly capitalizing on its strengths to generate and process broadband signals. By leveraging optical polarization and wavelength resources, spectral efficiency can be further enhanced, enabling high-capacity, high-resolution ISAC systems. Integrated waveform design promises a more compact ISAC architecture, though a comprehensive theoretical model to evaluate various metrics is still lacking. OFDM-based integrated waveforms feature a relatively better communication capability, yet further optimizations for microwave photonic applications are necessary. Integrated waveforms based on LFM have lower spectral efficiency, but they are useful for real-time and high-resolution imaging. Capitalizing on the benefits of integrated LFM waveforms in ISAC systems remains a pressing challenge. For practical applications in future 6G base stations, adaptive adjustment of ISAC parameters to suit various scenarios is necessary. Preliminary research has been conducted on resource allocation and parameter adjustment in the time and frequency domains. Further exploration is needed to maximize the benefits of microwave photonics. Based on the continuous efforts devoted to this interesting area, the deployment of microwave photonic ISAC systems can be expected in future 6G wireless networks.

ACKNOWLEDGMENT

The authors would like to thank the following individuals from the National Key Laboratory of Microwave Photonics, Nanjing University of Aeronautics and Astronautics, including but not limited to Qianwen Sang for contribution to Section I; Cong Ma and Shangzhe Xu for contribution to Section II; Zhenzhou Tang, Jijun He, and Zeyong Ding for contribution to Section II, Section III, and Section IV; and Zhouyang Pan, Xi Liu, and Haoran Wu for contribution to Section III.

REFERENCES

[1] *Framework and Overall Objectives of the Future Development of IMT for 2030 and Beyond*, Int. Telecommun. Union (ITU) Recommendation (ITU-R), Geneva, Switzerland, 2023.

[2] J. Struye et al., "Toward interactive multi-user extended reality using millimeter-wave networking," *IEEE Commun. Mag.*, vol. 62, no. 8, pp. 54–60, Aug. 2024.

[3] Z. Qadir, K. N. Le, N. Saeed, and H. S. Munawar, "Towards 6G Internet of Things: Recent advances, use cases, and open challenges," *ICT Exp.*, vol. 9, no. 3, pp. 296–312, 2023.

[4] X. Liu, H. Zhang, K. Sun, K. Long, and G. K. Karagiannidis, "AI-driven integration of sensing and communication in the 6G era," *IEEE Netw.*, vol. 38, no. 3, pp. 210–217, May 2024.

[5] M. Ghassemian et al., "Standardisation landscape for 6G robotic services," in *Proc. IEEE Conf. Standards Commun. Netw. (CSCN)*, Munich, Germany, Nov. 2023, pp. 148–154.

[6] M. H. Alsamh, A. Hawbani, S. Kumar, and S. H. Alsamhi, "Multi-sensory metaverse-6G: A new paradigm of commerce and education," *IEEE Access*, vol. 12, pp. 75657–75677, 2024.

[7] F. Dong, F. Liu, Y. Cui, W. Wang, K. Han, and Z. Wang, "Sensing as a service in 6G perceptive networks: A unified framework for ISAC resource allocation," *IEEE Trans. Wireless Commun.*, vol. 22, no. 5, pp. 3522–3536, May 2023.

[8] F. Liu et al., "Integrated sensing and communications: Toward dual-functional wireless networks for 6G and beyond," *IEEE J. Sel. Areas Commun.*, vol. 40, no. 6, pp. 1728–1767, Jun. 2022.

[9] F. Zhao et al., "A Ka-band 4TX/4RX dual-stream joint radar-communication phased-array CMOS transceiver," *IEEE Trans. Microw. Theory Techn.*, vol. 72, no. 3, pp. 1993–2008, Mar. 2024.

[10] M. Temiz, C. Horne, N. J. Peters, M. A. Ritchie, and C. Masouros, "An experimental study of radar-centric transmission for integrated sensing and communications," *IEEE Trans. Microw. Theory Techn.*, vol. 71, no. 7, pp. 3203–3216, Jul. 2023.

[11] J. Hecht, "The bandwidth bottleneck," *Nature*, vol. 536, no. 7615, pp. 139–142, 2016.

[12] S. Dang, O. Amin, B. Shihada, and M.-S. Alouini, "What should 6G be?" *Nature Electron.*, vol. 3, no. 1, pp. 20–29, Jan. 2020.

[13] S. Chen, Y. Liang, S. Sun, S. Kang, W. Cheng, and M. Peng, "Vision, requirements, and technology trend of 6G: How to tackle the challenges of system coverage, capacity, user data-rate and movement speed," *IEEE Wireless Commun.*, vol. 27, no. 2, pp. 218–228, Apr. 2020.

[14] J. Yao, "Microwave photonics," *J. Lightw. Technol.*, vol. 27, no. 3, pp. 314–335, Feb. 1, 2009.

[15] T. Berceli and P. R. Herczfeld, "Microwave photonics—A historical perspective," *IEEE Trans. Microw. Theory Techn.*, vol. 58, no. 11, pp. 2992–3000, Nov. 2010.

[16] W. Gou et al., "Photonic-based multiformat signal generator with dispersion immunity for multichannel transmission," *IEEE Trans. Microw. Theory Techn.*, vol. 72, no. 2, pp. 1280–1289, Feb. 2024.

[17] D. Marpaung, J. Yao, and J. Capmany, "Integrated microwave photonics," *Nature Photon.*, vol. 13, no. 2, pp. 80–90, Feb. 2019.

[18] J. Liu et al., "Photonic microwave generation in the X-and K-band using integrated soliton microcombs," *Nature Photon.*, vol. 14, no. 8, pp. 486–491, 2020.

[19] W. Zhang and J. Yao, "Photonic integrated field-programmable disk array signal processor," *Nature Commun.*, vol. 11, no. 1, p. 406, Jan. 2020.

[20] S. Li et al., "Chip-based microwave-photonic radar for high-resolution imaging," *Laser Photon. Rev.*, vol. 14, no. 10, Aug. 2020, Art. no. 1900239.

[21] J. Li, S. Yang, H. Chen, X. Wang, M. Chen, and W. Zou, "Fully integrated hybrid microwave photonic receiver," *Photon. Res.*, vol. 10, no. 6, p. 1472, 2022.

[22] A. Pizzinat, P. Chanclou, F. Saliou, and T. Diallo, "Things you should know about fronthaul," *J. Lightw. Technol.*, vol. 33, no. 5, pp. 1077–1083, Mar. 1, 2015.

[23] K. T. Truong and R. W. Heath Jr., "The viability of distributed antennas for massive MIMO systems," in *Proc. 47th Asilomar Conf. Signals, Syst. Comput.*, Pacific Grove, CA, USA, Nov. 2013, pp. 1318–1323.

[24] E. Park, S.-R. Lee, and I. Lee, "Antenna placement optimization for distributed antenna systems," *IEEE Trans. Wireless Commun.*, vol. 11, no. 7, pp. 2468–2477, Jul. 2012.

[25] D. Wang, C. Zhang, Y. Du, J. Zhao, M. Jiang, and X. You, "Implementation of a cloud-based cell-free distributed massive MIMO system," *IEEE Commun. Mag.*, vol. 58, no. 8, pp. 61–67, Aug. 2020.

[26] S. Jia et al., "0.4 THz photonic-wireless link with 106 Gb/s single channel bitrate," *J. Lightw. Technol.*, vol. 36, no. 2, pp. 610–616, Jan. 15, 2018.

[27] R. Igarashi et al., "First demonstration of 128-Gbit/s 300-GHz-band THz transmission using OFC-based transmitter and intradyne receiver," in *Proc. 27th OptoElectron. Commun. Conf. (OECC) Int. Conf. Photon. Switching Comput. (PSC)*, Jul. 2022, pp. 1–3.

[28] C. Liu, C. Wang, W. Zhou, F. Wang, M. Kong, and J. Yu, "81-GHz W-band 60-Gbps 64-QAM wireless transmission based on a dual-GRU equalizer," *Opt. Exp.*, vol. 30, no. 2, pp. 2364–2377, Jan. 2022.

[29] W. Li et al., "Photonics millimeter wave bidirectional full-duplex communication based on polarization multiplexing," *Opt. Lett.*, vol. 47, no. 24, pp. 6389–6392, Dec. 2022.

[30] Y. Horst et al., "Transparent optical-THz-optical link transmission over 5/115 m at 240/190 Gbit/s enabled by plasmonics," in *Proc. Opt. Fiber Commun. Conf. Exhib. (OFC)*, San Francisco, CA, USA, Jun. 2021, pp. 1–3.

[31] W. Tong et al., "Demonstration of 200-m wireless transmission in photonics-aided terahertz 2 × 2 MIMO system utilizing MRC technology for OFDM signals," *IEEE Trans. Microw. Theory Techn.*, early access, Dec. 9, 2024, doi: 10.1109/TMTT.2024.3507832.

[32] C.-C. Wei, Z.-X. Xie, P.-H. Ting, Z.-W. Huang, and C.-T. Lin, "3×3 MIMO 60-GHz OFDM-RoF system with long-distance wireless transmission enabled by MIMO Volterra filtering," *J. Lightw. Technol.*, vol. 40, no. 20, pp. 6860–6866, Oct. 15, 2022.

[33] H. Zhang et al., "Single-lane 200 Gbit/s photonic wireless transmission of multicarrier 64-QAM signals at 300 GHz over 30 m," *Chin. Opt. Lett.*, vol. 21, no. 2, 2023, Art. no. 023901.

[34] J. Ding et al., "THz-over-fiber transmission with a net rate of 5.12 Tbps in an 80 channel WDM system," *Opt. Lett.*, vol. 47, no. 12, p. 3103, 2022.

[35] X. Li, Y. Xu, and J. Yu, "Over 100-Gb/s V-band single-carrier PDM-64QAM fiber-wireless-integration system," *IEEE Photon. J.*, vol. 8, no. 5, pp. 1–7, Oct. 2016.

[36] Y. Cai et al., "Photonics-aided exceeding 200-Gb/s wireless data transmission over outdoor long-range 2 × 2 MIMO THz links at 300 GHz," *Opt. Exp.*, vol. 32, no. 19, pp. 33587–33602, 2024.

[37] X. Li et al., "1-Tb/s millimeter-wave signal wireless delivery at D-band," *J. Lightw. Technol.*, vol. 37, no. 1, pp. 196–204, Jan. 15, 2019.

[38] C. Zhang et al., "Clone-comb-enabled high-capacity digital-analogue fronthaul with high-order modulation formats," *Nature Photon.*, vol. 17, no. 11, pp. 1000–1008, Nov. 2023.

[39] C. Zhang et al., "High-fidelity sub-petabit-per-second self-homodyne fronthaul using broadband electro-optic combs," *Nature Commun.*, vol. 15, no. 1, p. 6621, Aug. 2024.

[40] Y. Zhu et al., "1-Pb/s CPRI-equivalent rate coherent DA-RoF fronthaul with 1024-QAM scalable in capacity, reach, and linewidth using residual carrier-based phase tracking," in *Proc. Asia Commun. Photon. Conf./Int. Photon. Optoelectronics Meetings (ACP/POEM)*, Wuhan, China, Nov. 2023, pp. 1–5.

[41] H. Ji, C. Sun, and W. Shieh, "Spectral efficiency comparison between analog and digital RoF for mobile fronthaul transmission link," *J. Lightw. Technol.*, vol. 38, no. 20, pp. 5617–5623, Oct. 15, 2020.

[42] D. Dodane et al., "Optical phase-locked loop phase noise in 5G mm-wave OFDM ARoF systems," *Opt. Commun.*, vol. 526, Jan. 2023, Art. no. 128872.

[43] K. Kale, R. Praveen, and Savita, "Phases distortion investigation in beyond 5G mm-wave OFDM," in *Proc. Int. Conf. Power Energy, Environ. Intell. Control (PEEIC)*, Gujrat, Pakistan, Dec. 2023, pp. 893–897.

[44] M. Noweir et al., "Digitally linearized radio-over fiber transmitter architecture for cloud radio access network's downlink," *IEEE Trans. Microw. Theory Techn.*, vol. 66, no. 7, pp. 3564–3574, Jul. 2018.

[45] H. J. Park, I. H. Ha, and S.-K. Han, "Linearization of multiband OFDM RoF system employing frequency-separated model based digital predistortion," *Opt. Commun.*, vol. 444, pp. 160–164, Aug. 2019.

[46] D. Zhu, J. Chen, and S. Pan, "Linearized phase-modulated analog photonic link with the dispersion-induced power fading effect suppressed based on optical carrier band processing," *Opt. Exp.*, vol. 25, no. 9, p. 10397, 2017.

[47] D. Zhu, J. Chen, and S. Pan, "Multi-octave linearized analog photonic link based on a polarization-multiplexing dual-parallel Mach–Zehnder modulator," *Opt. Exp.*, vol. 24, no. 10, p. 11009, 2016.

[48] G. Xu, J. Liu, W. Liu, Y. Chen, T. Liu, and S. Zhong, "Analog predistorter for RoF fronthaul link excited by a 400MHz bandwidth 5G NR signal," *IEEE Trans. Circuits Syst. II, Exp. Briefs*, vol. 71, no. 8, pp. 3975–3979, Aug. 2024.

[49] X. Zhang, S. Saha, R. Zhu, T. Liu, and D. Shen, "Analog pre-distortion circuit for radio over fiber transmission," *IEEE Photon. Technol. Lett.*, vol. 28, no. 22, pp. 2541–2544, Nov. 26, 2016.

[50] M. Noweir, M. Helaoui, D. Oblak, W. Chen, and F. M. Ghannouchi, "Linearization of radio-over-fiber cloud-RAN transmitters using pre- and post-distortion techniques," *IEEE Photon. Technol. Lett.*, vol. 33, no. 7, pp. 339–342, Apr. 12, 2021.

[51] Z. Cheng, X. Zhang, and G. Xu, "Low complexity digital predistortion for multiband radio over fiber systems," *IEEE Microw. Wireless Technol. Lett.*, vol. 34, no. 7, pp. 955–958, Jul. 2024.

[52] L. A. M. Pereira, L. L. Mendes, C. J. A. B. Filho, and A. C. Sodre, "Amplified radio-over-fiber system linearization using recurrent neural networks," *J. Opt. Commun. Netw.*, vol. 15, no. 3, pp. 144–154, Mar. 2023.

[53] P. Li et al., "One-shot blind frequency-domain nonlinear equalization for millimeter-wave fiber-wireless IFoF mobile fronthaul system," *J. Lightw. Technol.*, vol. 41, no. 14, pp. 4624–4634, Feb. 10, 2023.

[54] Y. Cai et al., "Large-capacity photonics-assisted millimeter-wave wireless communication enabled by dual-polarized SISO link and advanced MIMO equalizer," *J. Lightw. Technol.*, vol. 42, no. 11, pp. 4048–4059, Apr. 3, 2024.

[55] F. S. Shawqi, L. Audah, A. T. Hammoodi, M. M. Hamdi, and A. H. Mohammed, "A review of PAPR reduction techniques for UFMC waveform," in *Proc. 4th Int. Symp. Multidisciplinary Stud. Innov. Technol. (ISMSIT)*, Istanbul, Turkey, Oct. 2020, pp. 1–6.

[56] C. Huang et al., "Neural-network-based carrier-less amplitude phase modulated signal generation and end-to-end optimization for fiber-terahertz integrated communication system," *Opt. Exp.*, vol. 32, no. 6, p. 8623, 2024.

[57] S. Xu, J. Zhang, R. Yang, C. Li, and L. Yang, "RF mismatches and nonlinear distortions in cell-free massive MIMO: Impact analysis and calibration performance analysis," *IEEE Trans. Commun.*, vol. 72, no. 12, pp. 7526–7541, Dec. 2024.

[58] S. Xu, Z. Zhang, Y. Xu, C. Li, and L. Yang, "Deep reciprocity calibration for TDD mmWave massive MIMO systems toward 6G," *IEEE Trans. Wireless Commun.*, vol. 23, no. 10, pp. 13285–13299, Oct. 2024.

[59] J. Liu et al., "W-band RoF polarization multiplexing system supports 1048576 QAM with delta-sigma modulation," *Opt. Lett.*, vol. 48, no. 11, p. 2873, 2023.

[60] M. U. Hadi, H. Jung, P. A. Traverso, and G. Tartarini, "Experimental evaluation of real-time sigma-delta radio over fiber system for fronthaul applications," *Int. J. Microw. Wireless Technol.*, vol. 13, no. 8, pp. 756–765, Oct. 2021.

[61] L. Breyne, G. Torfs, X. Yin, P. Demeester, and J. Bauwelinck, "Comparison between analog radio-over-fiber and sigma delta modulated radio-over-fiber," *IEEE Photon. Technol. Lett.*, vol. 29, no. 21, pp. 1808–1811, Nov. 1, 2017.

[62] I. C. Sezgin et al., "A low-complexity distributed-MIMO testbed based on high-speed sigma-delta-over-fiber," *IEEE Trans. Microw. Theory Techn.*, vol. 67, no. 7, pp. 2861–2872, Jul. 2019.

[63] M. F. Keskin, I. C. Sezgin, H. Bao, H. Wymeersch, and C. Fager, "Localization with distributed MIMO using a high-speed sigma-delta-over-fiber testbed," *IEEE Microw. Wireless Compon. Lett.*, vol. 32, no. 7, pp. 923–926, Jul. 2022.

[64] L. Aabel, S. Jacobsson, M. Coldrey, F. Olofsson, G. Durisi, and C. Fager, "A TDD distributed MIMO testbed using a 1-bit radio-over-fiber fronthaul architecture," *IEEE Trans. Microw. Theory Techn.*, vol. 72, no. 10, pp. 6140–6152, Oct. 2024.

[65] B. Wang, M. Jian, F. Gao, G. Y. Li, and H. Lin, "Beam squint and channel estimation for wideband mmWave massive MIMO-OFDM systems," *IEEE Trans. Signal Process.*, vol. 67, no. 23, pp. 5893–5908, Dec. 2019.

[66] Y. Chen, Y. Xiong, D. Chen, T. Jiang, S. X. Ng, and L. Hanzo, "Hybrid precoding for wideband millimeter wave MIMO systems in the face of beam squint," *IEEE Trans. Wireless Commun.*, vol. 20, no. 3, pp. 1847–1860, Nov. 2020.

[67] F. Gao, L. Xu, and S. Ma, "Integrated sensing and communications with joint beam-squint and beam-split for mmWave/THz massive MIMO," *IEEE Trans. Commun.*, vol. 71, no. 5, pp. 2963–2976, May 2023.

[68] X. Ye, F. Zhang, and S. Pan, "Optical true time delay unit for multi-beamforming," *Opt. Exp.*, vol. 23, no. 8, pp. 10002–10008, 2015.

[69] X. Ye, D. Zhu, Y. Zhang, S. Li, and S. Pan, "Analysis of photonics-based RF beamforming with large instantaneous bandwidth," *J. Lightw. Technol.*, vol. 35, no. 23, pp. 5010–5019, Oct. 12, 2017.

[70] B. Paul, K. Sertel, and N. K. Nahar, "Photonic beamforming for 5G and beyond: A review of true time delay devices enabling ultra-wideband beamforming for mmWave communications," *IEEE Access*, vol. 10, pp. 75513–75526, 2022.

[71] C. Zhu et al., "Silicon integrated microwave photonic beamformer," *Optica*, vol. 7, no. 9, pp. 1162–1170, 2020.

[72] Q. Zhang et al., "Two-dimensional phased-array receiver based on integrated silicon true time delay lines," *IEEE Trans. Microw. Theory Techn.*, vol. 71, no. 3, pp. 1251–1261, Mar. 2023.

[73] N. K. Srivastava, R. Parihar, and S. K. Raghuwanshi, "Efficient photonic beamforming system incorporating a unique featured tunable chirped fiber Bragg grating for application extended to the Ku-band," *IEEE Trans. Microw. Theory Techn.*, vol. 68, no. 5, pp. 1851–1857, May 2020.

[74] N. M. Tessema et al., "A tunable Si_3N_4 integrated true time delay circuit for optically-controlled K-band radio beamformer in satellite communication," *J. Lightw. Technol.*, vol. 34, no. 20, pp. 4736–4743, Jun. 27, 2016.

[75] G. Choo, C. K. Madsen, S. Palermo, and K. Entesari, "Automatic monitor-based tuning of an RF silicon photonic 1X4 asymmetric binary tree True-Time-Delay beamforming network," *J. Lightw. Technol.*, vol. 36, no. 22, pp. 5263–5275, Sep. 30, 2018.

[76] Y. Liu et al., "Ultra-Low-Loss silicon nitride optical beamforming network for wideband wireless applications," *IEEE J. Sel. Topics Quantum Electron.*, vol. 24, no. 4, pp. 1–10, Jul. 2018.

[77] M. Huang, S. Li, M. Xue, L. Zhao, and S. Pan, "Flat-top optical resonance in a single-ring resonator based on manipulation of fast- and slow-light effects," *Opt. Exp.*, vol. 26, no. 18, pp. 23215–23220, 2018.

[78] M. Huang, S. Li, Z. Yang, and S. Pan, "Analysis of a flat-top optical ring resonator," *Opt. Commun.*, vol. 451, pp. 290–295, Nov. 2019.

[79] M. Morant, A. Trinidad, E. Tangdiongga, T. Koonen, and R. Llorente, "Experimental demonstration of mm-wave 5G NR photonic beamforming based on ORRs and multicore fiber," *IEEE Trans. Microw. Theory Techn.*, vol. 67, no. 7, pp. 2928–2935, Jul. 2019.

[80] I. Visscher et al., "Broadband true time delay microwave photonic beamformer for phased array antennas," in *Proc. 13th Eur. Conf. Antennas Propag. (EuCAP)*, Krakow, Poland, Mar. 2019, pp. 1–5.

[81] J. Fu, X. Chen, and S. Pan, "A fiber-distributed multistatic ultra-wideband radar," in *Proc. 14th Int. Conf. Opt. Commun. Netw. (ICOCN)*, Nanjing, China, Jul. 2015, pp. 1–3.

[82] T. Yao, D. Zhu, D. Ben, and S. Pan, "Distributed MIMO chaotic radar based on wavelength-division multiplexing technology," *Opt. Lett.*, vol. 40, no. 8, p. 1631, 2015.

[83] W. Feng et al., "Pulsed-chaos MIMO radar based on a single flat-spectrum and delta-like autocorrelation optical chaos source," *Opt. Exp.*, vol. 30, no. 4, pp. 4782–4792, 2022.

[84] Q. Guo, F. Zhang, P. Zhou, and S. Pan, "Dual-band LFM signal generation by optical frequency quadrupling and polarization multiplexing," *IEEE Photon. Technol. Lett.*, vol. 29, no. 16, pp. 1320–1323, Jun. 30, 2017.

[85] J. Zhang, O. L. Coutinho, and J. Yao, "A photonic approach to linearly chirped microwave waveform generation with an extended temporal duration," *IEEE Trans. Microw. Theory Techn.*, vol. 64, no. 6, pp. 1947–1953, Jun. 2016.

[86] Z. Yi, J. Wo, B. Mo, Y. Qiao, J. Zhang, and J. Yao, "Generation of a long linearly chirped microwave waveform based on a Fourier domain mode-locked optoelectronic oscillator incorporating a frequency shifting loop," *IEEE Trans. Microw. Theory Techn.*, vol. 72, no. 3, pp. 1911–1918, Mar. 2024.

[87] X. Ye, F. Zhang, Y. Yang, and S. Pan, "Photonics-based radar with balanced I/Q de-chirping for interference-suppressed high-resolution detection and imaging," *Photon Res.*, vol. 27, no. 3, pp. 265–272, Mar. 2019.

[88] Z. Tang and S. Pan, "A reconfigurable photonic microwave mixer using a 90° optical hybrid," *IEEE Trans. Microw. Theory Techn.*, vol. 64, no. 9, pp. 3017–3025, Sep. 2016.

[89] F. Zhang et al., "Photonics-based broadband radar for high-resolution and real-time inverse synthetic aperture imaging," *Opt. Exp.*, vol. 25, no. 14, pp. 16274–16281, Jul. 2017.

[90] X. Wang, F. Cao, C. Ma, Y. Yang, F. Zhang, and S. Pan, "Dual-band coherent microwave photonic radar using linear frequency modulated signals with arbitrary chirp rates," *IEEE J. Sel. Topics Quantum Electron.*, vol. 29, no. 6, pp. 1–9, Nov. 2023.

[91] G. Li, D. Shi, L. Wang, M. Li, N. Zhu, and W. Li, "Photonic system for simultaneous and unambiguous measurement of angle-of-arrival and Doppler-frequency-shift," *J. Lightw. Technol.*, vol. 40, no. 8, pp. 2321–2328, Apr. 15, 2022.

[92] Z. Kong et al., "Photonic approach for unambiguous measurement of AOA and DFS with self-interference cancellation," *IEEE Photon. Technol. Lett.*, vol. 35, no. 18, pp. 982–985, Jul. 6, 2023.

[93] Y. Yang, Z. Tang, Z. Xu, C. Yu, and S. Pan, "Microwave omnidirectional angle-of-arrival measurement based on an optical ten-port receiver," *J. Lightw. Technol.*, vol. 39, no. 23, pp. 7455–7463, Sep. 27, 2021.

[94] H. Zhuo, A. Wen, and Y. Wang, "Photonic angle-of-arrival measurement without direction ambiguity based on a dual-parallel Mach–Zehnder modulator," *Opt. Commun.*, vol. 451, pp. 286–289, Nov. 2019.

[95] H. Chen and E. H. W. Chan, "Angle-of-arrival measurement system using double RF modulation technique," *IEEE Photon. J.*, vol. 11, no. 1, pp. 1–10, Feb. 2019.

[96] C. Huang and E. H. W. Chan, "Multichannel microwave photonic based direction finding system," *Opt Exp.*, vol. 28, no. 17, pp. 25346–25357, Aug. 2020.

[97] H. Chen and E. H. W. Chan, "Simple approach to measure angle of arrival of a microwave signal," *IEEE Photon. Technol. Lett.*, vol. 31, no. 22, pp. 1795–1798, Nov. 15, 2019.

[98] H. Chen and E. H. W. Chan, "Photonics-based CW/pulsed microwave signal AOA measurement system," *J. Lightw. Technol.*, vol. 38, no. 8, pp. 2292–2298, Apr. 15, 2020.

[99] T. Yao, D. Zhu, S. Liu, F. Zhang, and S. Pan, "Wavelength-division multiplexed fiber-connected sensor network for SLource localization," *IEEE Photon. Technol. Lett.*, vol. 26, no. 18, pp. 1874–1877, Jul. 15, 2014.

[100] J. Fu, F. Zhang, D. Zhu, and S. Pan, "Fiber-distributed ultra-wideband radar network based on wavelength reusing transceivers," *Opt. Exp.*, vol. 26, no. 14, pp. 18457–18469, 2018.

[101] Q. Sun, J. Dong, C. Liu, J. Yang, X. Zhang, and W. Li, "Scalable distributed microwave photonic MIMO radar based on a bidirectional ring network," *Opt. Exp.*, vol. 29, no. 20, p. 31508, 2021.

[102] C. Ma et al., "Distributed microwave photonic MIMO radar with accurate target position estimation," *IEEE Trans. Microw. Theory Techn.*, vol. 71, no. 4, pp. 1711–1719, Apr. 2023.

[103] R. Li et al., "PFDIR—A wideband photonic-assisted SAR system," *IEEE Trans. Aerosp. Electron. Syst.*, vol. 59, no. 4, pp. 4333–4346, Apr. 2023.

[104] S. Peng et al., "High-resolution W-band ISAR imaging system utilizing a logic-operation-based photonic digital-to-analog converter," *Opt. Exp.*, vol. 26, no. 2, pp. 1978–1987, Jan. 2018.

[105] X. Zhang, H. Zeng, J. Yang, Z. Yin, Q. Sun, and W. Li, "Novel RF-source-free reconfigurable microwave photonic radar," *Opt. Exp.*, vol. 28, no. 9, p. 13650, 2020.

[106] C. Ma et al., "High-resolution microwave photonic radar with sparse stepped frequency chirp signals," *IEEE Trans. Geosci. Remote Sens.*, vol. 60, 2022, Art. no. 2007010.

[107] Y. Liu, Z. Zhang, M. Burla, and B. J. Eggleton, "11-GHz-bandwidth photonic radar using MHz electronics," *Laser Photon. Rev.*, vol. 16, no. 4, Apr. 2022, Art. no. 2100549.

[108] Z. Mo et al., "Microwave photonic de-chirp receiver for breaking the detection range swath limitation," *Opt. Exp.*, vol. 29, no. 7, p. 11314, 2021.

[109] F. Berland et al., "Microwave photonic MIMO radar for short-range 3D imaging," *IEEE Access*, vol. 8, pp. 107326–107334, 2020.

[110] G. Sun, Y. Zhou, Y. He, X. Yu, F. Zhang, and S. Pan, "Photonics-based MIMO radar with broadband digital coincidence imaging," *IEEE Trans. Microw. Theory Techn.*, vol. 72, no. 12, pp. 6996–7003, Dec. 2024.

[111] J. Dong, F. Zhang, Z. Jiao, Q. Sun, and W. Li, "Microwave photonic radar with a fiber-distributed antenna array for three-dimensional imaging," *Opt. Exp.*, vol. 28, no. 13, p. 19113, 2020.

[112] J. Ding, D. Zhu, Y. Yang, Z. Pan, and S. Pan, "Photonics-based multidomain features extraction for radio frequency signals," *IEEE Trans. Microw. Theory Techn.*, vol. 72, no. 6, pp. 3692–3700, Jun. 2024.

[113] X. Zou, H. Chi, and J. Yao, "Microwave frequency measurement based on optical power monitoring using a complementary optical filter pair," *IEEE Trans. Microw. Theory Techn.*, vol. 57, no. 2, pp. 505–511, Feb. 2009.

[114] S. T. Winnall, A. C. Lindsay, M. W. Austin, J. Canning, and A. Mitchell, "A microwave channelizer and spectroscope based on an integrated optical Bragg-grating Fabry–Pérot and integrated hybrid Fresnel lens system," *IEEE Trans. Microw. Theory Techn.*, vol. 54, no. 2, pp. 868–872, Feb. 2006.

[115] J. Shi, F. Zhang, D. Ben, and S. Pan, "Photonics-based broadband microwave instantaneous frequency measurement by frequency-to-phase-slope mapping," *IEEE Trans. Microw. Theory Techn.*, vol. 67, no. 2, pp. 544–552, Feb. 2019.

[116] C. Wang and J. Yao, "Ultrahigh-resolution photonic-assisted microwave frequency identification based on temporal channelization," *IEEE Trans. Microw. Theory Techn.*, vol. 61, no. 12, pp. 4275–4282, Dec. 2013.

[117] B. Zhu, J. Tang, W. Zhang, S. Pan, and J. Yao, "Broadband instantaneous multi-frequency measurement based on a Fourier domain mode-locked laser," *IEEE Trans. Microw. Theory Techn.*, vol. 69, no. 10, pp. 4576–4583, Oct. 2021.

[118] J. Ding, D. Zhu, Y. Yang, B. Ni, C. Zhang, and S. Pan, "Simultaneous angle-of-arrival and frequency measurement system based on microwave photonics," *J. Lightw. Technol.*, vol. 41, no. 9, pp. 2613–2622, Jan. 13, 2023.

[119] Y. Yang et al., "Photonics-based simultaneous angle of arrival and frequency measurement system with multiple-target detection capability," *J. Lightw. Technol.*, vol. 39, no. 24, pp. 7656–7663, Jun. 8, 2021.

[120] D. Zhu and S. Pan, "Broadband cognitive radio enabled by photonics," *J. Lightw. Technol.*, vol. 38, no. 12, pp. 3076–3088, Jun. 15, 2020.

[121] D. Zhu et al., "Microwave photonic cognitive radar with a subcentimeter resolution," *IEEE Trans. Microw. Theory Techn.*, vol. 72, no. 9, pp. 5519–5529, Sep. 2024.

[122] G. Serafino et al., "A photonics-assisted multi-band MIMO radar network for the port of the future," *IEEE J. Sel. Topics Quantum Electron.*, vol. 27, no. 6, pp. 1–13, Nov. 2021.

[123] S. Maresca et al., "Coherent MIMO radar network enabled by photonics with unprecedented resolution," *Opt. Lett.*, vol. 45, no. 14, pp. 3953–3956, 2020.

[124] F. Scotti, S. Maresca, L. Lembo, G. Serafino, A. Bogoni, and P. Ghelfi, "Widely distributed photonics-based dual-band MIMO radar for harbour surveillance," *IEEE Photon. Technol. Lett.*, vol. 32, no. 17, pp. 1081–1084, Jul. 29, 2020.

[125] Z. Zhang, Y. Liu, T. Stephens, and B. J. Eggleton, "Photonic radar for contactless vital sign detection," *Nature Photon.*, vol. 17, no. 9, pp. 791–797, Sep. 2023.

[126] J. Li, F. Zhang, Y. Xiang, and S. Pan, "Towards small target recognition with photonics-based high resolution radar range profiles," *Opt. Exp.*, vol. 29, no. 20, p. 31574, 2021.

[127] D. Kamissoko, J. He, H. Ganame, and M. Tall, "Performance investigation of W-band millimeter-wave radio-over-fiber system employing optical heterodyne generation and self-homodyne detection," *Opt. Commun.*, vol. 474, Nov. 2020, Art. no. 126174.

[128] X. Li, J. Xiao, Y. Xu, and J. Yu, "QPSK vector signal generation based on photonic heterodyne beating and optical carrier suppression," *IEEE Photon. J.*, vol. 7, no. 5, pp. 1–6, Oct. 2015.

[129] V. Torres-Company and A. M. Weiner, "Optical frequency comb technology for ultra-broadband radio-frequency photonics," *Laser Photon. Rev.*, vol. 8, no. 3, pp. 368–393, May 2014.

[130] J. Li, X. Yi, H. Lee, S. A. Diddams, and K. J. Vahala, "Electro-optical frequency division and stable microwave synthesis," *Science*, vol. 345, no. 6194, pp. 309–313, Jul. 2014.

[131] W. Li and J. Yao, "Investigation of photonically assisted microwave frequency multiplication based on external modulation," *IEEE Trans. Microw. Theory Techn.*, vol. 58, no. 11, pp. 3259–3268, Nov. 2010.

[132] L. Gao, W. Liu, X. Chen, and J. Yao, "Photonic-assisted microwave frequency multiplication with a tunable multiplication factor," *Opt. Lett.*, vol. 38, no. 21, p. 4487, 2013.

[133] Z. Tang, Y. Li, J. Yao, and S. Pan, "Photonics-based microwave frequency mixing: Methodology and applications," *Laser Photon. Rev.*, vol. 14, no. 1, Jan. 2020, Art. no. 1800350.

[134] Y. Gao, A. Wen, W. Zhang, W. Jiang, J. Ge, and Y. Fan, "Ultra-wideband photonic microwave I/Q mixer for zero-IF receiver," *IEEE Trans. Microw. Theory Techn.*, vol. 65, no. 11, pp. 4513–4525, Nov. 2017.

[135] Z. Tang, F. Zhang, and S. Pan, "60-GHz RoF system for dispersion-free transmission of HD and multi-band 16QAM," *IEEE Photon. Technol. Lett.*, vol. 30, no. 14, pp. 1305–1308, Jun. 8, 2018.

[136] S. Pan et al., "Satellite payloads pay off," *IEEE Microw. Mag.*, vol. 16, no. 8, pp. 61–73, Sep. 2015.

[137] H. Yuanzhi, T. Qinggui, W. Aijun, S. Lingyang, L. Yun, and S. Dongjuan, "Satellite communication payload based on microwave photonics: Benefits, architecture, and technologies," *IEEE Wireless Commun.*, vol. 31, no. 1, pp. 164–171, Feb. 2024.

[138] Z. Xue, S. Li, J. Li, X. Xue, X. Zheng, and B. Zhou, "OFDM radar and communication joint system using opto-electronic oscillator with phase noise degradation analysis and mitigation," *J. Lightw. Technol.*, vol. 40, no. 13, pp. 4101–4109, Mar. 7, 2022.

[139] W. Chen, D. Zhu, J. Liu, and S. Pan, "Multi-band RF transceiver based on the polarization multiplexed photonic LOs and mixers," *IEEE J. Sel. Topics Quantum Electron.*, vol. 27, no. 2, pp. 1–9, Mar. 2021.

[140] Y. Zhou, J. Kong, F. Zhang, and S. Pan, "Microwave photonic I/Q mixer for wideband frequency downconversion with serial electro-optical modulations," *Opt. Lett.*, vol. 49, no. 1, p. 65, Jan. 2024.

[141] T. Shi, D. Liang, M. Han, and Y. Chen, "Photonics-based de-chirping and leakage cancellation for frequency-modulated continuous-wave radar system," *IEEE Trans. Microw. Theory Techn.*, vol. 70, no. 9, pp. 4252–4262, Sep. 2022.

[142] S. Wang et al., "Photonic generation and de-chirping of broadband THz linear-frequency-modulated signals," *IEEE Photon. Technol. Lett.*, vol. 31, no. 11, pp. 881–884, Apr. 16, 2019.

[143] Y. Wang et al., "Photonics-assisted joint high-speed communication and high-resolution radar detection system," *Opt. Lett.*, vol. 46, no. 24, p. 6103, 2021.

[144] Y. Wang et al., "W-band simultaneous vector signal generation and radar detection based on photonic frequency quadrupling," *Opt. Lett.*, vol. 47, no. 3, pp. 537–540, Feb. 2022.

[145] M. Fang et al., "On-chip photonic MMW joint communication and radar system," in *Proc. Int. Topical Meeting Microw. Photon. (MWP)*, Nanjing, China, Oct. 2023, pp. 1–4.

[146] Y. Wang et al., "Integrated high-resolution radar and long-distance communication based-on photonic in terahertz band," *J. Lightw. Technol.*, vol. 40, no. 9, pp. 2731–2738, May 1, 2022.

[147] M. Lei et al., "Integrated wireless communication and mmW radar sensing system for intelligent vehicle driving enabled by photonics," in *Proc. 19th Int. Conf. Opt. Commun. Netw. (ICOCN)*, Qufu, China, Aug. 2021, pp. 1–3.

[148] R. Song and J. He, "OFDM-NOMA combined with LFM signal for W-band communication and radar detection simultaneously," *Opt. Lett.*, vol. 47, no. 11, pp. 2931–2934, Jun. 2022.

[149] J. Liang, J. He, R. Song, and Y. Xiao, "GS-16QAM OFDM with ANN scheme combined with LFM signal for joint communication and radar sensing system," *Opt. Lett.*, vol. 48, no. 13, p. 3459, 2023.

[150] Y. Wang, J. Liu, J. Ding, M. Wang, F. Zhao, and J. Yu, "Joint communication and radar sensing functions system based on photonics at the W-band," *Opt. Exp.*, vol. 30, no. 8, pp. 13404–13415, Apr. 2022.

[151] N. Zhong, P. Li, W. Bai, W. Pan, L. Yan, and X. Zou, "Spectral-efficient frequency-division photonic millimeter-wave integrated sensing and communication system using improved sparse LFM sub-bands fusion," *J. Lightw. Technol.*, vol. 41, no. 23, pp. 7105–7114, Dec. 1, 2023.

[152] M. Lei et al., "Demonstration of photonic sub-THz ISAC system with real-time 251.03-Gbps communication rate and offline 2.5-cm sensing resolution," in *Proc. 22nd Int. Conf. Opt. Commun. Netw. (ICOCN)*, Harbin, China, Jul. 2024, pp. 1–3.

[153] M. Lei et al., "A spectrum-efficient MoF architecture for joint sensing and communication in B5G based on polarization interleaving and polarization-insensitive filtering," *J. Lightw. Technol.*, vol. 40, no. 20, pp. 6701–6711, Oct. 15, 2022.

[154] S. Melo et al., "Dual-use system combining simultaneous active radar & communication, based on a single photonics-assisted transceiver," in *Proc. 17th Int. Radar Symp. (IRS)*, Krakow, Poland, May 2016, pp. 1–4.

[155] S. Jia et al., "A unified system with integrated generation of high-speed communication and high-resolution sensing signals based on THz photonics," *J. Lightw. Technol.*, vol. 36, no. 19, pp. 4549–4556, Aug. 6, 2018.

[156] Z. Lyu et al., "Multi-channel photonic THz-ISAC system based on integrated LFM-QAM waveform," *J. Lightw. Technol.*, vol. 42, no. 11, pp. 3981–3988, Apr. 22, 2024.

[157] Y. Men, J. Ji, A. Wen, Y. Wang, and F. Yang, "Photonic-assisted generation of joint radar and communication signals with immunity to power fading," *Opt. Commun.*, vol. 542, Sep. 2023, Art. no. 129598.

[158] X. Ge, F. Zhang, S. Pan, X. Hu, and C. Ma, "Photonic integrated sensing and communication system with multi-target detection capability," in *Proc. 14th Int. Photon. Optoelectron. Meetings (POEM)*, Wuhan, China, Apr. 2023, p. 63.

[159] X. Ge, F. Zhang, and S. Pan, "Photonic integrated wireless communication and sensing with OFDM modulation," in *Proc. Int. Academic Conf. Opt. Photon. (IACOP)*, Wuhan, China, Jan. 2024, p. 2.

[160] L. Huang, R. Li, S. Liu, P. Dai, and X. Chen, "Centralized fiber-distributed data communication and sensing convergence system based on microwave photonics," *J. Lightw. Technol.*, vol. 37, no. 21, pp. 5406–5416, Nov. 1, 2019.

[161] L. Peng, M. Yin, D. Zou, N. Yang, Y. Xiao, and F. Li, "Photonics-assisted integrated sensing and communication with ranging resolution improvement by multiple signal classification," *Opt. Exp.*, vol. 32, no. 20, p. 34796, 2024.

[162] F. Liu et al., "Millimeter-wave over fiber integrated sensing and communication system using self-coherent OFDM," *Opt. Exp.*, vol. 32, no. 9, p. 15493, 2024.

[163] J. Liu et al., "W-band photonics-aided OFDM system integrating sensing and communication with phase noise suppression scheme," *Opt. Laser Technol.*, vol. 180, Jan. 2025, Art. no. 111432.

[164] H. Yan et al., "W-band photonic-aided mm-wave ISAC system enabled by a shared OFDM signal waveform and a two-stage carrier frequency recovery algorithm," *Opt. Lett.*, vol. 49, no. 18, p. 5280, 2024.

[165] H. Nie, F. Zhang, Y. Yang, and S. Pan, "Photonics-based integrated communication and radar system," in *Proc. Int. Topical Meeting Microw. Photon. (MWP)*, Oct. 2019, pp. 1–4.

[166] Z. Lyu et al., "Radar-centric photonic terahertz integrated sensing and communication system based on LFM-PSK waveform," *IEEE Trans. Microw. Theory Techn.*, vol. 71, no. 11, pp. 5019–5027, Nov. 2023.

[167] S. Wang, D. Liang, and Y. Chen, "Photonics-assisted joint communication-radar system based on a QPSK-sliced linearly frequency-modulated signal," *Appl. Opt.*, vol. 61, no. 16, p. 4752, 2022.

[168] M. Lei et al., "Photonics-aided integrated sensing and communications in mmW bands based on a DC-offset QPSK-encoded LFMCW," *Opt. Exp.*, vol. 30, no. 24, pp. 43088–43103, Nov. 2022.

[169] Z. Lyu et al., "Preamble-free synchronization based on dual-chirp waveforms for photonic THz-ISAC," *J. Lightw. Technol.*, vol. 42, no. 8, pp. 2657–2665, Dec. 20, 2023.

[170] W. Bai et al., "Millimeter-wave joint radar and communication system based on photonic frequency-multiplying constant envelope LFM-OFDM," *Opt. Exp.*, vol. 30, no. 15, pp. 26407–26425, Jul. 2022.

[171] W. Bai et al., "Photonics-assisted millimeter-wave multiband integrated sensing and communication system using coherent receiving," *IEEE J. Sel. Topics Quantum Electron.*, vol. 29, no. 6, pp. 1–11, Nov. 2023.

[172] W. Bai et al., "Photonic super-resolution millimeter-wave joint radar-communication system using self-coherent detection," *Opt. Lett.*, vol. 48, no. 3, pp. 608–611, Feb. 2023.

[173] W. Bai et al., "Photonic millimeter-wave joint radar communication system using spectrum-spreading phase-coding," *IEEE Trans. Microw. Theory Techn.*, vol. 70, no. 3, pp. 1552–1561, Mar. 2022.

[174] Z. Xue, S. Li, X. Xue, X. Zheng, and B. Zhou, "Photonics-assisted joint radar and communication system based on an optoelectronic oscillator," *Opt. Exp.*, vol. 29, no. 14, pp. 22442–22454, Jul. 2021.

[175] A. K. Alzamil, M. A. Sharawy, E. M. Almohimmah, A. M. Ragheb, A. Almaiman, and S. A. Alshebeili, "Development of an integrated communication and sensing system using spread spectrum and photonics technologies," *Photonics*, vol. 11, no. 9, p. 861, Sep. 2024.

[176] T. Umezawa, K. Jitsuno, A. Kanno, K. Akahane, N. Yamamoto, and T. Kawanishi, "OFDM millimeter-wave radar experiment combined with radio over fiber technology," in *Proc. 41st Int. Conf. Infr., Millim., THz waves (IRMMW-THz)*, Copenhagen, Denmark, Sep. 2016, pp. 1–2.

[177] M. Li, T. Hao, W. Li, and Y. Dai, "Tutorial on optoelectronic oscillators," *APL Photon.*, vol. 6, no. 6, pp. 1–29, Jun. 2021.

[178] F. Zou et al., "Optoelectronic oscillator for 5G wireless networks and beyond," *J. Phys. D, Appl. Phys.*, vol. 54, no. 42, Oct. 2021, Art. no. 423002.

[179] M. Liu, S. Liu, L. Yang, C. Du, H. Liu, and S. Pan, "Improving the quality of arbitrary periodic waveform via injection-locking of an optoelectronic oscillator," *IEEE Trans. Microw. Theory Techn.*, vol. 72, no. 11, pp. 6678–6685, Nov. 2024.

[180] D. Eliyahu, D. Seidel, and L. Maleki, "Phase noise of a high performance OEO and an ultra low noise floor cross-correlation microwave photonic homodyne system," in *Proc. IEEE Int. Freq. Control Symp.*, Honolulu, HI, USA, May 2008, pp. 811–814.

[181] S. Pan and Y. Zhang, "Microwave photonic radars," *J. Lightw. Technol.*, vol. 38, no. 19, pp. 5450–5484, Oct. 1, 2020.

[182] D. Brunner et al., "Bistatic OFDM-based ISAC with over-the-air synchronization: System concept and performance analysis," *IEEE Trans. Microw. Theory Techn.*, early access, Nov. 8, 2024, doi: 10.1109/TMTT.2024.3487295.

[183] Z. Lyu et al., "Dual-chirp-based photonic THz-ISAC system with adaptive frequency synchronization," *Opt. Lett.*, vol. 49, no. 16, p. 4493, 2024.

[184] B. T. Brandão, J. H. Silva, L. S. Leitão, D. Castanheira, F. P. Guiomar, and P. P. Monteiro, "5G-NR based joint RADAR and communication system using low-cost photonic fronthaul," in *Proc. Int. Topical Meeting Microw. Photon. (MWP)*, Nov. 2021, pp. 1–4.

[185] B. Dong et al., "Photonic-based flexible integrated sensing and communication with multiple targets detection capability for W-band fiber-wireless network," *IEEE Trans. Microw. Theory Techn.*, vol. 72, no. 8, pp. 4878–4891, Aug. 2024.

[186] J. Jia, B. Dong, L. Tao, J. Shi, N. Chi, and J. Zhang, "Demonstration of radar-aided flexible communication in a photonics-based W-band distributed integrated sensing and communication system for 6G," *Chin. Opt. Lett.*, vol. 22, no. 4, 2024, Art. no. 043901.

[187] B. Dong et al., "Demonstration of photonics-based flexible integration of sensing and communication with adaptive waveforms for a W-band fiber-wireless integrated network," *Opt. Exp.*, vol. 30, no. 22, p. 40936, 2022.

[188] B. Dong et al., "Photonic-based W-band integrated sensing and communication system with flexible time-frequency division multiplexed waveforms for fiber-wireless network," *J. Lightw. Technol.*, vol. 42, no. 4, pp. 1281–1295, Jan. 15, 2024.

[189] J. Zhang and J. Yao, "Broadband microwave signal processing based on photonic dispersive delay lines," *IEEE Trans. Microw. Theory Techn.*, vol. 65, no. 5, pp. 1891–1903, May 2017.

[190] Y. Sun et al., "Field-programmable ring array employing AMZI-assisted-MRR structure for photonic signal processor," *APL Photon.*, vol. 9, no. 6, Jun. 2024, Art. no. 066104.

[191] H. Guillet de Chatellus, L. R. Cortés, and J. Azaña, "Optical real-time Fourier transformation with kilohertz resolutions," *Optica*, vol. 3, no. 1, pp. 1–8, Jan. 2016.

[192] B. Zhang et al., "Impact of dispersion effects on temporal-convolution-based real-time Fourier transformation systems," *J. Lightw. Technol.*, vol. 38, no. 17, pp. 4664–4676, May 11, 2020.

[193] D. Woods and T. J. Naughton, "Photonic neural networks," *Nature Phys.*, vol. 8, no. 4, pp. 257–259, 2012.

[194] K. Liao, T. Dai, Q. Yan, X. Hu, and Q. Gong, "Integrated photonic neural networks: Opportunities and challenges," *ACS Photon.*, vol. 10, no. 7, pp. 2001–2010, Jul. 2023.

[195] Y. Liu, A. Deng, S. Hua, S. Xu, and W. Zou, "Photonic ADC-based scheme for joint wireless communication and radar by adopting a broadband OFDM shared signal," *Opt. Lett.*, vol. 47, no. 20, p. 5421, 2022.

[196] A. Khilo et al., "Photonic ADC: Overcoming the bottleneck of electronic jitter," *Opt. Exp.*, vol. 20, no. 4, p. 4454, 2012.

[197] X. Jiang et al., "GNSS-over-fiber sensing system for high precision 3D nodal displacement and vibration detection," *IEEE Photon. Technol. Lett.*, vol. 35, no. 8, pp. 402–405, Mar. 2, 2023.

[198] L. Wang, L. Ren, X. Wang, and S. Pan, "Time-resolution enhanced multi-path OTD measurement using an adaptive filter based incoherent OFDR," *Chin. Opt. Lett.*, vol. 22, no. 1, 2024, Art. no. 013901.

[199] S. Pan, J. Wei, and F. Zhang, "Passive phase correction for stable radio frequency transfer via optical fiber," *Photonic Netw. Commun.*, vol. 31, no. 2, pp. 327–335, Apr. 2016.

[200] L. Wang, X. Wang, and S. Pan, "Time phase shifting based demodulation method for fast optical fiber transfer delay measurement," in *Proc. Int. Topical Meeting Microw. Photon. (MWP)*, Nanjing, China, Oct. 2023, pp. 1–3.

[201] L. Wang et al., "Speed-enhanced optical fiber transfer delay measurement based on digital phase detecting," in *Proc. Asia Commun. Photon. Conf. (ACP)*, Shanghai, China, Oct. 2021, pp. 1–3.

[202] X. Y. Xingwei Ye, B. Z. B. Zhang, Y. Z. Y. Zhang, D. Z. D. Zhu, and S. Pan, "Performance evaluation of optical beamforming-based wideband antenna array," *Chin. Opt. Lett.*, vol. 15, no. 1, 2017, Art. no. 010013.

[203] S. Xu et al., "Optical beamforming system based on polarization manipulation with amplitude–phase coupling suppression," *IEEE Trans. Microw. Theory Techn.*, vol. 71, no. 5, pp. 2215–2221, May 2023.

[204] P. Martinez-Carrasco, T. H. Ho, D. Wessel, and J. Capmany, "Ultra-broadband high-resolution silicon RF-photonic beamformer," *Nature Commun.*, vol. 15, no. 1, p. 1433, Feb. 2024.

[205] A. Li et al., "An integrated single-shot spectrometer with large bandwidth-resolution ratio and wide operation temperature range," *PhotoniX*, vol. 4, no. 1, p. 29, Sep. 2023.

[206] A. Raptakis et al., "Integrated heterodyne laser Doppler vibrometer based on stress-optic frequency shift in silicon nitride," *PhotoniX*, vol. 4, no. 1, p. 30, Sep. 2023.
[207] T. Chen, Z. Dang, Z. Deng, S. Ke, Z. Ding, and Z. Zhang, "Large-scale optical switches by thermo-optic waveguide lens," *PhotoniX*, vol. 5, no. 1, p. 14, Apr. 2024.
[208] L. Tang, Z. Tang, S. Li, S. Liu, and S. Pan, "Simultaneous measurement of microwave Doppler frequency shift and angle of arrival based on a silicon integrated chip," *IEEE Trans. Microw. Theory Techn.*, vol. 70, no. 9, pp. 4243–4251, Sep. 2022.
[209] D. W. Prather et al., "Fourier-optics based opto-electronic architectures for simultaneous multi-band, multi-beam, and wideband transmit and receive phased arrays," *IEEE Access*, vol. 11, pp. 18082–18106, 2023.
[210] T. Gong et al., "Holographic MIMO communications: Theoretical foundations, enabling technologies, and future directions," *IEEE Commun. Surveys Tuts.*, vol. 26, no. 1, pp. 196–257, 1st Quart., 2024.
[211] J. C. Deroba, G. J. Schneider, C. A. Schuetz, and D. W. Prather, "Multifunction radio frequency photonic array with beam-space down-converting receiver," *IEEE Trans. Aerosp. Electron. Syst.*, vol. 54, no. 6, pp. 2746–2761, Dec. 2018.

Lihan Wang received the B.S. degree from Nanjing University of Aeronautics and Astronautics, Nanjing, China, in 2020, where he is currently pursuing the Ph.D. degree at the National Key Laboratory of Microwave Photonics.

His research interests include microwave photonic measurements, integrated sensing and communications, and integrated fiber-wireless networks.

Xiangchuan Wang received the B.Eng. degree in automation and the Ph.D. degree in microelectronics and solid-state electronics from Nanjing University, Nanjing, China, in 2009 and 2015, respectively.

He is currently a Professor with the National Key Laboratory of Microwave Photonics, Nanjing University of Aeronautics and Astronautics, Nanjing. He has authored or coauthored over 80 research papers. His current research interests include microwave photonic measurement and optical fiber sensing technologies.

Shilong Pan (Fellow, IEEE) received the B.S. and Ph.D. degrees in electronics engineering from Tsinghua University, Beijing, China, in 2004 and 2008, respectively.

From 2008 to 2010, he was a "Vision 2010" Post-Doctoral Research Fellow with the Microwave Photonics Research Laboratory, University of Ottawa, Ottawa, ON, Canada. He joined the College of Electronic and Information Engineering, Nanjing University of Aeronautics and Astronautics, Nanjing, China, in 2010, where he is currently a Full Professor and the Executive Director of the National Key Laboratory of Microwave Photonics. His research focused on microwave photonics, which includes optical generation and processing of microwave signals, analog photonic links, photonic microwave measurement, and integrated microwave photonics.

Dr. Pan is a Fellow of IEEE, Optica, SPIE, and IET. He was selected as an IEEE Photonics Society Distinguished Lecturer in 2019 and an IEEE MTT-S Distinguished Microwave Lecturer in 2022. He was a recipient of the IEEE MTT-S Outstanding Young Engineer Award in 2021. He is currently the Deputy Editor of *Chinese Optics Letters*, an Associate Editor of the IEEE/OPTICA JOURNAL OF LIGHTWAVE TECHNOLOGY, and IEEE TRANSACTIONS ON MICROWAVE THEORY AND TECHNIQUES, and is the Vice Chair of IEEE MTT-22 Microwave Photonics. He was the Chair of a number of international conferences, symposia, and workshops, including the TPC Chair of the ICOCN 2015, the TPC Chair of IEEE MWP in 2023, the TPC Co-Chair of IEEE MWP 2017, and the General Co-Chair of IEEE MWP 2021.